Ray-tracing in non-radial envelopes of protostars

Bachelor Thesis

Author(s):
Baumann, Gisela

Publication date:
2006

Permanent link:
https://doi.org/10.3929/ethz-a-005226651

Eidgenössische Technische Hochschule Zürich
Swiss Federal Institute of Technology Zurich

Ray-tracing in non-radial envelopes of Protostars

Bachelor Thesis

presented by

Gisela Baumann

carried out under the guidance of Prof. Dr. A. Benz

at the Institute of Astronomy of the

SWISS FEDERAL INSTITUTE OF TECHNOLOGY ZURICH

between February 2006 and April 2006

submitted the 9th of May 2006

Contents

Abstract

AFGL 2591 is a newborn blue, highmassive protostar, with 3000 light years toward the constellation of Cygnus and an age of less than 10^5 years. Its luminosity is about 20'000 times that of the sun. The diameter of this giant star is of about 10 times the diameter of the sun. Its nebula from which AFGL 2591 is originated has actually 500 times the diameter of our Solar system. AFGL 2591 is a deeply embedded high-mass YSO - a high-mass protostellar object for which extensive observational data exists. Hence the envelope of AFGL 2591 is still collapsing, density and temperature fluctuate with time and are strongly increasing in the inner part of the protostar. After a certain time the protostar starts to emit radiation, which can be determined with help of the radiative transfer theory which I will explain later. First the protostar emits radiation in the infrared and later the wavelength are mostly in the range of X-rays.

This Radiation has a drastic influence on the chemical composition within the inner $10'000\,\mathrm{AU}$ of the protostar. As being successfully observed by the researcher group of Prof. Dr. Arnold Benz of ETH Zurich, the emission of radiation around AFGL 2591 is not spherically symmetrical as being assumed so far for the constructed models. The purpose was then now to imitate and extend a source model, which is already created by the researcher group of Floris van der Tak at University of Groningen: It assumes a cylindrical symmetry.

The received data determined by this model had to be adjusted to the observed data and the chemical models and then maps of the brightness temperature spectrum will be produced.

1 Introduction

The formation of stars begins with the collapse of a dense interstellar cloud core, a reservoir of gas and dust which form the source of protostars and circumstellar disks. A strongly radiating accretion shock front is then created by infalling cloud matter onto the star. Shock-generated photons heat the gas and destroy grains out to a radius of the order 0.1AU. The far-infrared continuum radiation is emitted by the accretion luminosity which diffuses through the dusty envelope. The high energy loss from the shocks finally leads to modest protostellar radii and later on, when the object has grown to a certain size and mass, convection takes place and nuclear reactions like deuterium fusion is ignited. [Stahler, Palla (2004)] Molecules are formed and deplete onto grains around the protostar, which later on may accumulate into stars or planetary bodies. Such grains are then called called ices.

In cold molecular cores prior to star formation the chemistry is dominated by low-temperature gas-phase reactions which leads to the formation of unsaturated molecules, small radicals and to the formation of the ices. For latter, surface reactions play a rather important role, since during the collapse phase the density becomes so high that most molecules accrete onto grains and are incorporated into an icy mantle. The primary constituents of the mantles and cores of the grains are H_2O ice and silicates. By the time the formation of the star is completed its radiation, being released when the star has collapsed enough to reach a ignition temperature of about 10^{-7} K, required for hydrogen fusion, heats up the surrounding envelope, that the molecules evaporate back into the gas phase. The evaporation depends on their binding energy. Additionally the outflows from the new star penetrate the envelope, creating high-temperature shocks and turbulent regions of low-temperature, returning volatile and refractory material. These evaporated molecules react in a periode of 10^5 years into different chemical processes. Some of the gas-phase and icy material can be aggregated through accretion into the circumstellar disk surrounding the young star.

It can be found, that carbon-rich molecules are more abundant in the diffuse outer part and NH_3 is more numerous in the dense cloud centre. But NH_3 is difficult to detect, because the N-H-features are blocked with deep H_2O ice bands. Depletion is very difficult to prove observationally, since every cloud has its own skin in which the abundances are normal [Mundy & McMullin (1997)] and which therefore masks any depletions deep inside the cloud.

Direct observations of ices indicate that the column density of solid CO is apparently comparable to that of gas-phase CO. During the phase of the cold collapsing envelope the density increases whereas temperature decreases.

From this results an enhanced depletion of gas-phase molecules in the envelope which causes a dust obscuration, avoiding direct observations of ices. But the interstellar ices have been detected in absorption by their vibrational bands in the infrared, embedded in young stars. The ices can be seen in the cold envelope in absorption due to high temperature difference to their surrounding dust, which is heated by the YSO's to a few hundreds Kelvin. YSO's are young stellar objects which have already dispersed their envelopes and cloud cores, so that no confusion with the surrounding material is possible. Other species with presumably theoretically high abundances are O_2 and N_2 but because they don't have an intrinsic dipole moment they are very hard to detect in the infrared.

How do interstellar ices form?

1. Surface chemistry of species accreted on interstellar grains
2. Thermal processing of ice mantles, where the heat is coming from nearby nearly fromed stars.
3. Energetic processing of ices by particles bombardment
4. Depletion of molecules produced in the gas phase and in shocks.

1.1 Molecular clouds - the origin of (proto-)stars

Molecular Cloud is a type of interstellar cloud. Interstellar matter consists of neutral and ionised gas as well as dust and cosmic rays. The creation of newborn stars occurs exclusively within molecular clouds. These objects lead to interstellar absorption. In the Milky Way the interstellar material consists of 90 % hydrogen, 10 % helium and the rest are metal traces. 99 % of the matter exists in gaseous form. The remaining one percent is dust. Neither density nor temperature of the interstellar matter are constant. The temperature range from 20 K up to a million Kelvin, depending on the location of the gas.

In molecular clouds temperatures from 20 K to 50 K and densities of $10^3 - 10^5$ atoms per cm^{-3} are detected.

Component	Temperature [K]	Density $[\frac{\text{atoms}}{\text{cm}^3}]$	State
GMC	7 - 15	100 - 300	
Molecular clouds	20 - 50	10^3 - 10^5	molecules
HI clouds	50 - 100	1 - 10^3	neutral atoms
HII regions	10^4	10^2 - 10^4	mostly ionised

where I means: not ionised or atomic gas and II means: ionised for instance p^+ and e^-

Almost 0.001 % of the molecular cloud are composed of other molecules, like carbon monoxide (CO), water (H_2O), hydrocyanic acid (HCN) or organic bonds.

Dark clouds are a special kind of molecular clouds. They are distinguished by being colder and smaller. Dark clouds are primarily heated by cosmic rays. [van Dishoeck et al. (1998)] The carbon monoxide is the most famous molecule of molecular clouds research due to the ratio $\frac{\mathrm{CO}}{\mathrm{H_2}}$ which determines the mass of such a cloud. The giant molecular clouds (GMC) have average densities of $100 - 300$ molecules per cm^2, as well as an inner temperature of $7 - 15\,\mathrm{K}$. The centre of the cloud is completely invisible in the visible wave range. But it can easily be seen in the microwave band, given that microwaves are less absorbed by the dust. These clouds exhibit a inner magnetic field.

1.2 Observational techniques

We know today, that half of the interstellar matter in our galaxy is in molecular from, primarily as H_2 molecules. [Genzel (1989)] Enormous gaseous clouds, reaching more than 10^6 times the solar mass, consist only of molecules and are the locations where new stars are born. The best way to accomplish observations of such a dense medium, is to do studies at infrared, submillimeter and radiowavelength.

At those wavelength thermal emissions from dust particles dominates. [Genzel, Burton, Elmegreen (1991)] Observations in the infrared reveal something about material absorption of young stars in our line of sight. Physical parameters can in most cases be determined by looking at the excitation temperature from the molecules in a certain region. Important molecules without a permanent dipole moment (like H_3^+, CO_2, CH_4, C_2H_2) possess strong infrared rovibrational transition, but negligible rotational emissions in the milimeter range. Therefore they are hardly detectable in the submilimeter range. The advantage of submilimeter data are that they are not restricted to absorption toward the infrared source. Additionally the spectral resolving power is much higher so that the line profiles are kinematically better resolved and provide information on the molecules locations.

1.3 General observational difficulties

- uncertainties in the excitation
- uncertainties in the optical depth of the lines
- unresolved source structure

O_2 is very difficult to observe owing to its extremely hyperfine splitting weak infrared bands [Ehrenfreund et al. 1992]. Also H_2 is not directly observable, except if it is in dense clouds. In HI clouds it is only possible to detect it, using radio telescopes. The hyperfine splitting of the hydrogen atom in its ground state between $J = 0$ and $J = 1$, J being the total angular momentum, leads to a spectral line with a wave length of 21.1 cm, which is a part of the radio spectrum with its 1420.4 MHz. Within a region of HI gas, a hydrogen atom can be excited by collisions with neighboring atoms to this excited state $J = 1$. Then there is a small probability that the downward transition occurs through emission of a 21.1 cm photon. But it's important that strong lines in a spectrum don't necessarily mean higher abundances of the observed molecule. This effect may also occur because of high temperatures or densities. [van Dishoeck et al. (1998)]

1.4 Interstellar chemistry [van Dishoeck et al. (1998)], [Mannings, Boss, Russel (2000)]

In the interstellar clouds we find a rich chemistry - with nearly 120 different molecules. Interstellar chemistry has been described successfully by ion-molecule gas-phase schemes, although not all effects can be explained. Therefore the gas-grain interactions and the grain-surface chemistry provided a certain assistance. [van Dishoeck et al. (1998)]

1.4.1 Gas-phase chemistry

Only two-body reactions are of importance at the low densities of interstellar clouds. Molecular bonds are formed by several different processes such as radiative association, photodissociation, dissociative recombination and ion-molecule reactions. The parameters used to create a truthfully model are mainly density, temperature, radiation field, initial elemental abundances and geometry [Millar et al. (1997)], [Lee et al. (1996)]. The density, temperature and the initial elemental abundances are based on observations, while the radiation field is typically parameterised in terms of a standard interstellar radiation field, diminished according to the depth. [Mannings, Boss, Russel (2000)] The most important heavy elements and their abundances in the gas-phase chemistry are carbon and oxygen in gaseous but also in atomic form. Despite the high quantities of H and H_2 the reactions with these two elements are limited to small ions due to high energy barriers for large ions and neutrals. In hot core regions and shocked gas the reactions:

$$O + H_2 \rightarrow OH \quad \text{and} \quad OH + H_2 \rightarrow H_2O \tag{1}$$

take place and drive oxygen into water above $\sim 230\,\mathrm{K}$ [Charnley 1997]. The removal from the radiation source of most neutral small molecules is limited by photodissociation at the edges of clouds or near young stars. Photodissociation can lead to radicals which can react to form other molecules. With larger distance to the radiation source destruction is mainly done by O and C^+ reactions. So we are interested in endothermic reactions like such involving sulfur. [van Dishoeck et al. (1998)]

1.4.2 Tracers

Often used as tracers of dense gas are the molecules HCO^+ and $H^{13}CO^+$.

For the pure gas-phase [Mannings, Boss, Russel (2000)] tracers are:

$$H_2 \; + \; \text{cosmic-ray ionisation} \rightarrow H_2^+ \tag{2}$$

$$H_2^+ \; + \; H_2 \rightarrow H_3^+ \; + \; H \tag{3}$$

$$H_3^+ \; + \; H \; + \; \text{atoms and molecules} \rightarrow \text{rich chemistry} \tag{4}$$

But the most important transition in the chemistry is the production of CO from neutral and ionised atomic carbon.

$$C^+ + H_2 \rightarrow CH^+C + H_3^+ \rightarrow COC + OH \rightarrow COC + O_2 \rightarrow CO \tag{5}$$

This is true for cloud densities of 10^4 - $10^5\,\mathrm{cm}^{-3}$. This process is so important because the creation of more complex organic species and carbon chains requires large abundances of C and C^+. O_2 is produced through the reaction of O and OH, but the abundances of such species are low at early times because OH, O_2 and H_2O willingly react with C and C^+. But all these chemical abundances do not necessarily reflect the age of the core since its formation of a diffuse gas exhibiting turbulences or outflows.

1.4.3 Grain-surface chemistry

The presence of H_2S in cold clouds indicates grain-surface chemistry processes. The surface of interstellar grains produces at low temperatures and densities hydrogenated species, due to the high mobility of atomic hydrogen on cold surfaces. With an increasing density the atomic oxygen reactions become more and more important (e. g. $CO + O \rightarrow CO_2$). At higher temperatures the diffusion of heavier species becomes significant. [van Dishoeck

et al. (1998)] Hydrogenation and oxidation are the dominating reactions on the grain surface.

Molecules accrete from the gas phase, where CO is the dominant C-bearing species. The key step in the surface chemistry of CO is hydrogenation to HCO which reacts on a grain with H and may form complex species. To test models of grain surface chemistry observations of hot cores near massive stars are made, where the ices have evaporated off the grains. The frequent surface reaction of O and H to form H_2O can be blocked if the atomic O reacts with CO on a grain. [Mannings, Boss, Russel (2000)]

1.4.4 Processing by ultraviolet photons

When the ice mantle is heated to a temperature near its sublimation point, outgassings occur. (Thermal processing) UV photolysis of ices containing H_2O CO, NH_3 and CH_4 produces small reactive radicals such as H, O, OH, N, NH, NH_2, C, CH, CH_3 and CH_2, which react with each other and form different species like H_2O_2 or CO_2.

The further chemistry is much akin to the surface hydrogenation scheme for CO which runs through HCO, as it is mentioned in the grain surface chemistry above. So the two chemical processes give rise to obviously the same species. The differences of these two schemes are; in the surface chemistry scheme the relative abundances reflect the relative accretion rates of the migrating radicals H, C, N and O [Tielens, Hagen (1982)], while the photolysis scheme (gas phase chemistry) is convolved with the UV destruction rate of the parent species.

1.5 Chemical models

The gas raining onto the protostar originates from the outer envelope. The gas temperature rises with the density as a result of efficient heating by dust. As the infalling gas continues to be compressed, the radiation eventually becomes trapped by the high opacity from the grains. There is a dust photosphere at a radius of 10^{14} cm inside which the temperature rises much more quickly. This radius defines the effective radiating surface of the protostar, which can be seen by an observer for instance on earth. Another boarder around protostars is the dust envelope, being the region that is opaque to the protostar's radiation. If the temperature rises above 1500 K all hot grains vaporise. The temperature depends on the adopted grain model. (See chapter: Gas-grain models)

1.5.1 Gas-phase models

Pure gas models are most successful in reproducing the observed abundances at early times (10^4 years) in GMC's. To calculate the chemical abundances in dense clouds it is required to know some parameters such as temperature, density and radiation field. There are two models existing:

1. steady-state: The abundances of the molecules do not change with time but are depth-dependant, e. g. ultraviolet photon- or X-ray-dominated regions near young stars [Hollenbach & Tielens (1989)]

2. time-dependant: The abundances are depth-independent, but change with time, e. g. models of hot cores near massive young stars.

Both models take in account the element abundances of C, O, N, S, metals etc. and the ionisation rate of primary cosmic-rays.

The additional parameters for these models are:
For a):

- geometry
- density $n_H = n(H) + 2n(H_2)$
- incident radiation field
- grain parameters (such as extinction curve)
- the temperature-position function of gas and dust

For b):

- density (time-dependant)
- visual extinction-position function
- temperature is often set at 10 K for gas *and* dust

The main characteristics of these two models are the transition of carbon from atomic to molecular form. In model a) C^+ recombines to C followed by the conversion to CO. The presence of atomic carbon is essential to build up more complex organic molecules and long carbon chains. These atoms are abundant only at early times.

It is important that chemical composition determines the cooling rates and that the dynamical and chemical time scales are comparable, even if researchers do not succeed in putting these two models into one.

In pseudo-time-dependant models the density is taken to be constant with time. For instance the models appropriate for hot cores is one of these models. There the temperatures are much higher and the initial composition of the gas is taken to be molecular instead of atomic for consistency reason of the composition of evaporating ice mantles in the vicinity of young stars.

1.5.2 Gas-grain models

For gas densities of more than $10^4 \frac{1}{\mathrm{cm}^3}$ all gas molecules (except a few weakly polar molecules) should accrete onto grain surfaces in 10^4 years, which is a timescale comparable to the timescale for protostar formation. It is complicated by the fact, that molecules that freeze onto grain surfaces can be reinjected into the gas phase by the desorption of grain mantles.

Mainly there are two different gas-grain models [Tielens, Charnley (1997)]:

The accretion-limited regime:
[Tielens, Hagen (1982)] Reactions are limited by the rate at which species are dispensed to the grain surface where they immediately migrate and react.This is used for the grain-surface chemistry.

The reaction-limited regime:
[Hasegawa, Herbst (1993)], [Hasegawa, Herbst (1993)] Many reactive species are present on a grain surface. The reaction is controlled by surface concentrations. This regime is used in most of the gas-grain interaction-models.

A rather essential point of the gas-grain model is the mechanism for returning the molecules to the gas phase. If we forget about the desorption the gas molecules accrete onto the grains surfaces in $\frac{2 \cdot 10^9}{n_H \cdot y_S}$ year, where y_S is the sticking coefficient $= 0.1 - 1.0$. As a consequence in a typical dark cloud (with density of $10^4 \frac{1}{\mathrm{cm}^3}$) most molecules should disappear from the gas phase within 10^6 years. This is a contradiction to the observations what implies the presence of the desorption mechanisms even in cold clouds. (The energy liberated by the formation of molecules heats the grains locally and may remove some of them.) The correctness of such mechanisms depend on binding energies of the molecules on the surface. Polar molecules such as H_2O which contain strong hydrogen bonds in the ices, are difficult to remove from the surface whereas nonpolar molecules such as N_2 have low binding energies and therefore can easily be returned to the gas phase.

1.6 Envelopes - Models of envelopes of high-mass YSO's

YSO's are strong emitters of X-rays. This radiation may affect the physical and chemical structure of their surroundings. An enhancement of the ionisation rate accelerates the formation of molecules while for higher ionisation rates, H_2 is destroyed as well as other molecules.

Compared to low-mass YSO's, the temperature is higher in high-mass YSO's over a large part of the envelope, and the cores may also be heated externally by nearby young stars. The ice mantle compositions are dependant on the temperature and density in collapsing envelopes. The density profile results in a steep gradient in the gas phase $\frac{H}{CO}$ ratio:

At *low densities* of $< 5 \cdot 10^3 \frac{1}{\mathrm{cm}^3}$ the atomic hydrogen abundance in the gas is high and most of all heavy elements accrete as atoms, leading to polar H_2O, CH_4 and NH_3 ices.

Then at *intermediate densities* of about $10^4 - 10^5 \frac{1}{\mathrm{cm}^3}$, most of the gas phase carbon is tied up as CO. Consequently, the accreted CO may react with small amounts of atomic hydrogen to give CO_2.

At *high densities* ($> 5 \cdot 10^3 \frac{1}{\mathrm{cm}^3}$) most of the oxygen and nitrogen are in the form of O_2 and N_2 as gas. Layered ices can be produced in a collapsing envelope, wherein the polar ices condense first and the nonpolar species froming a volatile grain crust. It has to be noticed, that all desorption mechanisms are much more efficient for volatile species (CO, O_2, N_2) than for nonvolatile materials like H_2O, CH_3OH... It follows from the temperature gradient in the envelope that in the evaporation of the volatile ices components like CO, CO_2 have temperatures in the inner part of above 20 K to 45 K respectively.

1.6.1 Observations of envelopes around high-mass YSO's

The ice mantle composition is remarkably simple, formed by hydrogenation and oxidation of O, N, C and CO. Major species that are expected to be present in the ices but that cannot be observed are O_2, N_2 and NH_3. The ices toward high-mass objects have a smaller fraction of nonpolar CO than the low-mass cases. The clear variations in the gas/solid ratio of CO_2 indicates the development of a hot core in the inner envelope in which the ices are evaporated and where the high temperatures drive the gas phase oxygen into H_2O.

1.7 Chemistry

1.7.1 Influence of development of protostars on chemistry

When an ice mantle is heated to a temperature near its sublimation point, outgassings occur. Star formation in molecular clouds was detected by observing the widespread outflows of supersonic (meaning with speed over the speed of sound) gas. It is due to the angular momentum which has to be disposed of the collapsing cloud core, that material of high velocity is ejected from young stars. The reason for the observed non-isotropic outflows is still debated whether collimated jets or winds are responsible. [Pelletier & Pudritz (1992)], [Shu et al. (1995)] Anyway, the high-velocity material flows outward and strikes the envelope. Shocks are driven into the originally quiescent material, thus new chemical processes may occur.

The chemical details of these shocks depend on whether the shocks are of the J(jump) or C(continuous) type [Draine & McKee (1993)], [Hollenbach (1997)]. The peak temperature of C shocks are typically $2000-3000\,\mathrm{K}$ which is too low for molecular dissociation to occur. In J shocks the temperature is increased to very high values ($10^5\,\mathrm{K}$) such that all molecules are dissociated [Hollenbach & McKee (1989)], [Neufeld & Dalgarno (1989a)], [Neufeld & Dalgarno (1989b)]. Additionally ultraviolet radiation is produced, which may photodissociate molecules both in and ahead of the shocks. But most often a mixture of J- and C-type shocks occurs. They affect the grain cores and their mantles.

Observation shows that the cloud structure appears to be completely dominated by the outflows, passing the entire region and thereby sweep up material and shockcompress the gas. The outflow interaction zone or more precisely its chemical composition may be used to estimate the products of grain mantle chemistry. One of the prime predictions of all shock models is then, that in dense clouds there is a copious production of H_2O, which contains all oxygen not locked up in CO. Therefore we have high H_2O abundances of at least 10^{-5}. H_2O contributes the total cooling of the object.

1.7.2 Chemistry in the cold collapse envelopes around deeply embedded YSO's

When a collapse occurs, the increasing density and decreasing temperature accelerates the gas-phase depletion of molecules onto grain mantles, while the radiative heating and outflow from the central star act to return molecules into the gas phase.

In the outer region of the collapsing envelope (bigger than $10^{16}\,\mathrm{cm}$) the temperature remains low owing to the efficient cooling by the molecules. It

can be assumed that in those regions the temperature is almost constantly 10 K.

There are certain models with very high dust temperatures in the inner region. They assume, that gas is heated by collisions with the warm dust, by compressional heating and by absorption of infrared photons such as the gas achieve the same temperature as this inner region. Hot dust, heated up to 100 K at radii of $< 10^{15}$ cm produce a sublimation of H_2O-rich ices into the gas, as well as a convertion of O and O_2 into H_2O, once the gas is heated to $200 - 300$ K. This changes the chemistry in the inner part, but there is little information about that yet.

If we assume in a model that only thermal desorption has to be taken in account, all species condense, except H_2 and perhaps N_2. N_2H^+ and HCO^+ remain also high because the H_3^+ abundance increases when its main removal partners (CO, O, H_2O...) are condensed onto grains. A good tracer of the collapsing envelopes are these ions.

The envelope around a YSO can be heated by ultraviolet photons generated in the inner boundary layer between the fast rotating accretion disk and the much slower rotating protostar. [Hartigan et al. (1991)] These ultraviolet photons can escape through the cavity evacuated by the outflow and be scattered by dust grains into the envelope. [Spaans et al. (1995)] To observe the envelope around low-mass YSO's one could look at the ice mantles through infrared absorption, but at the earliest stages, the dust obscuration is so high that the source is not visible even at mid-infrared wavelengths. At a more evolved stage, it becomes possible to probe the ice mantles surrounding such objects. More powerful indicators of physical and chemical processes taking place in the collapsing envelope are line profiles. [Rawlings et al. (1992)] An excellent tracer of the envelope structure and mass is HCO^+. It's abundance does not decrease in the innermost regions. N_2H^+, on the other hand, seems to trace the quiescent outer envelope gas in low-mass YSO's [Bachiller (1996)], [Mardones et al. 1997].

1.7.3 Chemistry in prestellar cores

NH_3 was found to be more abundant in older cores where stars have already formed. Prestellar cores have a relatively flat density distribution on scales of $0.02 - 0.05$ pc. H_2O, CO and CO_2 are detected at abundances that indicate that up to 40% of the heavy elements may be frozen out at densities of a few times $10^4 \frac{1}{\mathrm{cm}^3}$. The amount of solid CO is comparable to that of gas-phase CO. The chemical composition at several positions away from the YSO show remarkably uniform abundances in contrast with dark cores.

1.7.4 Chemistry in hot cores [van Dishoeck et al. (1998)]

Heating its inner envelope, the young star is surrounded by radiation or shocks to temperatures above $\sim 100\,\mathrm{K}$, followed by a distinctive chemically rich phase. These are called hot cores. They are small ($< 0.1\,\mathrm{pc}$), dense ($n(\mathrm{H_2}) > 10^6\,\frac{1}{\mathrm{cm}^3}$) and warm ($T_K > 100\,\mathrm{K}$). Most of them have associated masers [Shepherd & Churchwell (1996)], [Acord et al. (1997)] and show signs of active outflows. They usually can be found near HII regions [Wood & Churchwell (1989)] and are characterised by high abundances of fully hydrogenated molecules such as $\mathrm{H_2O}$,
[Gensheimer et al. (1996)], $\mathrm{NH_3}$ [Genzel et al. (1982)], [Pauls et al. (1983)] and $\mathrm{H_2S}$ [Minh et al. (1990)], [Minh et al. (1991)] along with a rich variety of complex organic molecules.

Hot cores can be studied through infrared absorption line observations. [Mitchell et al. (1990)], [van Dishoeck et al. (1998)]

Observations of hot cores may provide tighter constraints on the composition and complexity of the minor species in grain mantles. The observed abundances of hot cores molecules are much larger than can be produced by low-temperature ion-molecule gas phase chemistry. The best model nowadays is the one, which chemistry is driven by the evaporation of icy grain mantles. There are two classes of reactions that break down the evaporated molecules and initiate the hot core chemistry:

1. Reaction with hydrogen:

$$H_2S + H \rightarrow SH + H_2 \tag{6}$$

2. Reactions with protonated molecules which are followed by dissociative recombination:

$$H_2O + H_3^+ \rightarrow H_3O^+ \tag{7}$$

$$H_3O^+ + e \rightarrow OH \text{ or } O \tag{8}$$

At $T \geq 230\,\mathrm{K}$ most of the oxygen is driven into $\mathrm{H_2O}$ and almost no O and $\mathrm{O_2}$ are available. Three kinds of species can be distinguished in hot cores, according to the models;

1. Molecules that are produced in the precollapse, cold dense cloud chemistry by ion-molecule reactions and later on frozen onto grains and released into the gas phase largely unaltered.

2. Molecules that are made by grain-surface reactions and then released into the gas

3. Molecules that are produced by the rapid gas phase chemistry in the hot core between evaporated molecules.

Not as in all recent developed models, the hot core is embedded in an extended envelope or halo with varying density and temperature. And its time scale is determined by the rate at which the first-generation molecule react, which is the species described in 2). This strongly depends on the temperature of the gas and the ionisation fraction. Compared to the observed abundances it leads to an estimated age of hot core reactions, which should be close to that of the YSO. The age of the orion compact ridge W3 (H_2O) is estimated to be $\sim 6'000$ years old [Charnley 1997]. And object G34.3+0.15 is approximately $3000 - 10'000$ years old [Millar et al. (1997)]. The ages of the envelopes in which hot cores are embedded are typically 10^5 years. The difference of time between envelopes and hot cores agrees remarkably well with the dynamical times estimated for the outflows. Many cores actually contains YSO's.

It can be possible that hot cores are fragmented into clumps and are dispersed at later times, due to expansion of HII region, photoevaporation, winds and outflows. Some parts of the hot core material may also end up in new stars. But once the hot core is dispersed, the ultraviolet radiation from the young massive star can affect the surrounding envelope by setting up a neutral photon-dominated-region outside the HII region.

1.8 Radiative transfer [Rybicki, Lightman (1979)]

We can consider a small cylinder [Karttunen et al. (2001)], whose bottom has an area dA and a length of ds and the intensity in the solid angle $d\Omega$ is I_ν [Wm^{-2} Hz^{-1} ster^{-1}]. If dI is the intensitychange of the radiation during passing the distance dr, the energy change inside the cylinder in time dt is:

$$dE = dI_\nu \cdot dA \cdot d\nu \cdot d\Omega \cdot dt \tag{9}$$

This is equal to the emission minus absorption that takes place inside the cylinder. [Karttunen et al. (2001)] So it is the energy crossing dA in time dt and frequency range $d\nu$. [Rybicki, Lightman (1979)] The absorbed energy is:

$$dE_{abs} = \alpha_\nu \cdot I_\nu \cdot ds \cdot dA \cdot d\nu \cdot d\Omega \cdot dt \tag{10}$$

where α_ν is the absorption coefficient, a character for the opacity of the medium at frequency ν. The absorption coefficient α_ν, in units of $[\frac{1}{cm}]$ represents the loss of intensity in a beam as it travels a distance ds. It is defined as

$$dI_\nu = -\alpha_\nu \cdot I_\nu \cdot ds \tag{11}$$

where $\alpha_\nu = \rho \cdot \kappa_\nu$ and ρ is the mass density and κ_ν is also called the opacity coefficient. I_ν is the intensity at frequency ν along a particular line of sight parameterised by ds.

On the other hand the energy emitted in the solid angle $d\Omega$ in the cylinder is:

$$dE_{em} = j_\nu \cdot ds \cdot dA \cdot d\nu \cdot d\Omega \cdot dt \tag{12}$$

where j_ν is in the units of [erg $\cdot$ cm^{-3} s^{-1} ster^{-1} Hz^{-1}]. Thus we can define the relation between emissivity and the spontaneous emission coefficient j,

$$j_\nu = \frac{\varepsilon_\nu \cdot \rho}{4\pi} \tag{13}$$

only holding for isotropic emission. So the emission coefficient is defined as the energy which is emitted per unit time per unit solid angle and per unit volume:

$$\begin{aligned} dE_{em} &= j_\nu \cdot dV \cdot d\Omega \cdot dt \cdot d\nu \\ &= \varepsilon_\nu \cdot \rho \cdot dV \cdot dt \cdot d\nu \cdot \frac{d\Omega}{4\pi} \end{aligned}$$

where ε = emissivity, ρ = mass density of the emitted medium, $d\Omega$ is the solid angle and j_ν = the emitted energy divided by volume unit and time unit at frequency ν in a solid angle $d\Omega$. This is only true for a isotropic emitter. The intensity added to the beam by spontaneous emission is:

$$dI_\nu = j_\nu \cdot ds \tag{14}$$

In many cases α_ν and j_ν will depend on the local mean intensity of the radiation field. Therefore we define the mean intensity J_ν:

$$J_\nu = \frac{1}{4\pi} \int d\Omega \; I_\nu \, . \tag{15}$$

So, J_ν is the average intensity received from all solid angles $d\Omega$, and I_ν is the solution of the following radiative transport equation (See (17)) along each direction under consideration. [Hogerheijde, van der Tak, (2000)] To obtain the total radiation density u we can simply integrate over all frequencies [Rybicki, Lightman (1979)]:

$$u = \frac{4\pi}{c} \int J_\nu \; d\nu \, . \tag{16}$$

The true absorption as well as the simulated emission are proportional to the intensity of the incoming beam. The combined expression for emission and absorption is: $dE = -dE_{abs} + dE_{em}$ [Karttunen et al. (2001)] and thus

$$\frac{dI_\nu}{ds} = -\alpha_\nu \cdot I_\nu + j_\nu \,. \tag{17}$$

This incorporates most macroscopic aspects of radiation into one equation.

In the limiting case of $\alpha_\nu = 0$:

$$\frac{dI_\nu}{ds} = j_\nu \tag{18}$$

with the solution:

$$I_\nu(s) = I_\nu(s_0) + \int_{s_0}^{s} j_\nu(s')\; ds' \,. \tag{19}$$

This means that if there is no absorption, the increase in brightness is equal to the emission coefficient integrated along the line of sight.

In the case of $j_\nu = 0$ the equation becomes

$$\frac{dI_\nu}{ds} = -\alpha_\nu \cdot I_\nu \tag{20}$$

with the solution

$$I_\nu(s) = I_\nu(s_0) \cdot \exp\Big(\int_{s_0}^{s} j_\nu(s')\; ds'\Big) \,. \tag{21}$$

It can be seen, that for this case where only absorption is present, the brightness decreases along the ray by the exponential of the absorption coefficient integrated along the line of sight.

$$\boxed{\frac{dI_\nu}{ds} = -\alpha_\nu \cdot I_\nu + j_\nu} \tag{22}$$

This is called the *transfer equation*. It can be simplified by introducing the optical depth and the source function: The optical depth along a path of a travelling ray is defined by

$$d\tau_\nu = \alpha_\nu \cdot ds \tag{23}$$

or

$$d\tau_\nu(s) = \int_{s_0}^{s} \alpha_\nu(s')\; ds' \,. \tag{24}$$

A medium is said to be *optically thick* or *opaque* if $\tau_\nu > 1$. And a medium is *optically thin* or *transparent* for $\tau_\nu < 1$. The absorbance increase by the

thickness of the medium. After introducing the structure function, which is the ratio between the emission coefficient and the absorption coefficient,

$$S_\nu = \frac{j_\nu}{\alpha_\nu} \tag{25}$$

because of 1.8, our transfer equation can be written as:

$$\boxed{\frac{dI_\nu}{d\tau_\nu} = -I_\nu + S_\nu} \tag{26}$$

which is the fundamental *equation of radiative transport*. The formal solution of the transfer equation is:

$$I_\nu(\tau_\nu) = I_\nu(0) \cdot e^{-\tau_\nu} + \int_0^{\tau_\nu} e^{-(\tau_\nu - \tau'_\nu)}\ S_\nu(\tau'_\nu)\ d\tau'_\nu \tag{27}$$

where the first term can be interpreted as the initial intensity diminished by absorption and the second term is the integrated source diminished by absorption. If

$$\frac{dI_\nu}{d\tau_\nu} = 0 \tag{28}$$

the emission in a volume unit is as great as the absorbed energy. That is called the *thermodynamical equilibrium* and it is in that state where the body radiates like a blackbody. So then the source function is equal to the Planck function [Karttunen et al. (2001)]:

$$S_\nu = B_\nu(T) = \frac{2h\nu^3}{c^2} \cdot \frac{1}{e^{\frac{h\nu}{kT}} - 1}\,. \tag{29}$$

We consider [Hogerheijde, van der Tak, (2000)] both molecules and dust particles as sources of emission and absorption

$$j_\nu = j_\nu(\text{dust}) + j_\nu(\text{gas}) \quad \text{and} \quad \alpha_\nu = \alpha_\nu(\text{dust}) + \alpha_\nu(\text{gas}) \tag{30}$$

but ignore scattering, because scattering effects are usually negligible at wavelengths longer than mid-infrared.

For thermal continuum emission for dust, $j_\nu(\text{dust})$ and $\alpha_\nu(\text{dust})$ are simply given by [Hogerheijde, van der Tak, (2000)]:

$$j_\nu(\text{dust}) = \alpha_\nu(\text{dust}) \cdot B_\nu(T_{\text{dust}}) \tag{31}$$

where B_ν is the Planck function (29) at the dust temperature T_{dust} and

$$\alpha_\nu(\text{dust}) = \kappa_\nu \cdot \rho_{\text{dust}} \tag{32}$$

where κ_ν is the dust opacity in cm^{-2} per unit (dust) mass and ρ_{dust} is the mass density of the dust. [Hogerheijde, van der Tak, (2000)] So we treat the dust as a blackbody.

For the gaseous part of the emission and absorption we need to look at the spectral lines to determine $\alpha_\nu^{uk}(\mathrm{gas})$ and $j_\nu^{uk}(\mathrm{gas})$. The absorption and emission between level u and k set these two parameters. They are strongly peaked around ν_0 with a frequency dependence described by a line-profile function $\Phi(\nu)$ as will be seen later in this text.

$$j_\nu^{uk}(gas) = \frac{h\nu_0}{4\pi}\ n_u\ A_{uk}\ \Phi(\nu) \tag{33}$$

$$\alpha_\nu^{uk} = \frac{h\nu_0}{4\pi}\ (n_k\ B_{ku} - n_u\ B_{uk})\ \Phi(\nu) \tag{34}$$

where n_u and n_k are the populations on the energy levels u and k, determined by collision and radiation. According to M. R. Hogerheijde and F. F. S. van der Tak, in most interstellar clouds the line profile is dominated by Doppler broadening due to the turbulent velocity field as can be seen from our calculations later.

$$\Phi(\nu) = \frac{c}{b\nu_0\sqrt{\pi}}\ \exp\Big(-\frac{c^2(\nu-\nu_0)^2}{\nu_0^2 b^2}\Big) \tag{35}$$

where b is the full width of the Gaussian.

If we then add a velocity field the line-profile becomes angle-dependent and the local velocity vector $(\nu - \nu_0)$ enters. In the end the intensity flux J_ν contains parts of the CMB, dust and spectral lines, which themselves depend on the level populations through (33) and (34) together with the equation of radiative transport (1.8). Therefore the problem must be solved iteratively or in case of rarely varying physical conditions an approximate value of J_ν can be found from the local conditions. [Hogerheijde, van der Tak, (2000)]

1.8.1 The Einstein coefficients

Einstein identified three processes by looking at the absorption of a photon of energy $h\nu_0$ emitted in a transition from the energy level $E + h\nu_0$ to E.

1. Spontaneous emission: Occurs even in the absence of a radiation field; the system drops from the higher energy level to a lower one by emitting a photon. The Einstein A-coefficient is A_{21} = Transition probability per unit time for spontaneous emission $[\frac{1}{\mathrm{s}}]$.

2. Absorption: The system makes a transition by absorbing a photon. Since there is no self-interaction of the radiation field, we expect that there is a proportionality between the density of photons at frequency ν_0 and the probability per unit time. To be precise it should be taken in account, that the energy difference between the two levels is not sharp, but described by a line profile function $\Phi(\nu)$ which determines the line shape.

3. Simulated emission: This process is caused by the emission of a photon.

In the thermodynamic equilibrium the number of transitions per unit time per unit volume *out* of state 1 must be the same as the number of transitions per unit time per unit volume *into* state 1. So there is a relation between all Einstein coefficients which is equal to the Planck-function

$$B_\nu(\tau) = \frac{\frac{2h\nu^3}{c^2}}{e^{\frac{h\nu}{kT}} - 1} \tag{36}$$

for all temperatures:

$$g_1 B_{12} = g_2 B_{21} A_{21} = \frac{2h\nu^3}{c^2} \cdot B_{21} \tag{37}$$

where A_{21}, B_{12}, B_{21}, represent the atomic properties; the Einstein coefficients. There is no temperature included in these equations thus it must hold whether or not the atoms are in thermodynamic equilibrium. As a short remark it should be noted, that if we neglect the stimulated emission, then we obtain the Wien law because $h\nu \gg kT$ and therefore the number densities of atoms in level 1 and 2, n_1 and n_2 are not comparable: $n_2 \ll n_1$. Also for emission the coefficient is proportional to the intensity and only affects the photons along the given beam, in analogy to the process of absorption. So we treat simulated emission as negative absorption, and we get the absorption coefficient expressed in microscopic quantities of the Einstein-B-coefficient.

$$\frac{\alpha_\nu}{4\pi} \cdot \Phi(\nu) \cdot (n_1 B_{12} - n_2 B_{21}) \tag{38}$$

where the line shape function $\Phi(\nu)$ gives the probability that a photon is emitted at frequency interval $[\nu, \nu + d\nu]$ and $\int \Phi(\nu) d\nu = 1$. So it is simpler to speak of the absorption coefficient when also taking in account the correction for stimulated emission. The transfer equation finally becomes:

$$\frac{dI_\nu}{ds} = -\frac{h\nu}{4\pi} \cdot (n_1 B_{12} - n_2 B_{21})\ \Phi(\nu)\ I_\nu + \frac{h\nu}{4\pi} n_2\ A_{21}\ \Phi(\nu) \tag{39}$$

and the source function

$$S_\nu = \frac{n_2\ A_{21}}{n_1\ B_{12} - n_2\ B_{21}} \tag{40}$$

Using the Einstein coefficients the absorption coefficient can then be written:

$$\alpha_\nu = \frac{h\nu}{4\pi} \cdot n_1 \cdot B_{12} \cdot (1 - \frac{g_1 n_2}{g_2 n_1}) \cdot \Phi(\nu)\,. \tag{41}$$

If the matter is in thermal equilibrium with itself but not necessarily with the radiation, we have :

$$\frac{n_1}{n_2} = \frac{g_1}{g_2}\ e^{\frac{-h\nu}{kT}} \tag{42}$$

where T is the excitation temperature. In this case

$$\alpha_\nu = \frac{h\nu}{4\pi} \cdot n_1 B_{12}[1 - e^{\frac{-h\nu}{kT}}]\ \Phi(\nu) \tag{43}$$

and $S_\nu = B_\nu(T)$ is the blackbody radiation field at temperature T. The coefficient $1 - e^{\frac{-h\nu}{kT}}$ is due to stimulated emission.

$$B_\nu(T) = \frac{2h\nu^3}{c^2} \cdot \frac{1}{e^{\frac{h\nu}{kT}} - 1} \tag{44}$$

with the solution

$$I_\nu = B_\nu(T_{ex}(1 - e^{-\tau_\nu}) + I_\nu^{\text{brightness}}\ e^{-\tau_\nu} \tag{45}$$

[Rybicki, Lightman (1979)]

If $S_\nu(\tau_{\nu)}$ is constant inside the interstellar dust and background radiation is neglected, we get

$$I_\nu = S_\nu \int_0^{\tau_\nu} e^{-(\tau_\nu - \tau_{\nu'})}\ d\tau_{\nu'} = S_\nu\ (1 - e^{-\tau_\nu}) \tag{46}$$

and if the interstellar dust or cloud is optically thick which means $\tau_\nu \gg 1$ then $I_\nu = S_\nu$. So there is a equilibrium between absorption and emission processes. [Karttunen et al. (2001)] τ_ν is the optical depth and the brightness is meant to be the intensity received at the antenna. We define the brightness temperature by the relation $I_\nu = B_\nu(T_b)$. In radio astronomy where the Rayleigh-Jeans law is usually applicable we can write:

$$I_\nu = \frac{2\nu^2}{c^2} \cdot kT_b \tag{47}$$

If we write the transfer equation of thermal emission in terms of brightness temperature in the Rayleigh-Jeans approximation we receive:

$$\frac{T_R}{d\tau_\nu} = -T_{\text{brightness}} + T \tag{48}$$

where T is the excitation temperature, being equal to the temperature of the material. This Rayleigh-Jeans equation give us the relation between the measured spectral radiation and the surface temperature. It actually results from the Planck formula which has been developed in a Taylor expansion. It is important to mention, that the brightness temperature is a function of ν, except to the case where the source is a blackbody. If T is constant we have:

$$T_{\text{brightness}} = T_{\text{background}} \cdot e^{-\tau_\nu} + T\ (1 - e^{-\tau_\nu}) \tag{49}$$

if

$$h\nu \ll kT\,.$$

To discuss the collision rates we establish the rates C_{ij} as the collision rates per second per molecule of the species of interest. These coefficients depend on the density of the collisional analogs to the Einstein relations:

$$n_1\ C_{12} = n_2\ C_{21} \tag{50}$$

and therefore

$$C_{12} = \frac{g_2}{g_1} \cdot C_{21}\ e^{-\frac{\Delta E}{kT}} \tag{51}$$

which must hold also in cases out of equilibrium. We write now the statistical equilibrium for two levels:

$$\frac{dn_1}{dt} = -n_1(B_{12}\overline{J} + C_{12}) + n_2(A_{21} + B_{21}\overline{J} + C_{21}) + n_2(A_{21} + B_{21}\overline{J} + C_{21}) \tag{52}$$

$$\frac{dn_2}{dt} = n_2(B_{12}\overline{J} + C_{12}) - n_2(A_{21} + B_{21}\overline{J} + C_{21}) \tag{53}$$

where $\overline{J} = \int_0^\infty J_\nu \Phi(\nu) d\nu$ and J_ν is the averaged I_ν over 4π steradian. To solve these equations we must make assumptions:

The first idea comes from Sobolev to invent a factor that determines the chance that a photon at some position in the cloud can escape the system. So $\overline{J}$ comes from the inside radiation of the source. If β is the chance that a newly created photon can escape from the cloud, then $\overline{J} = S(1 - \beta)$, thus

$$\frac{dn_2}{dt} = (n_1 C_{12} - n_2 C_{21}) - \beta n_2 A_{21}\,. \tag{54}$$

That was the goal, to separate the level population from the radiation field. The estimation for our escape probability is established on the assumption, that β depends on geometry and the optical depth but *not* on the radiation field. In the one dimensional case:

$$\beta = \langle e^{-\tau} \rangle = \frac{1}{\tau} \int_0^\tau e^{-\tau'} \, d\tau' = \frac{1 - e^{-\tau}}{\tau} \,. \tag{55}$$

For a homogeneous slab one can find:

$$\beta = \frac{1 - e^{-3\tau}}{3\tau} \,. \tag{56}$$

For a uniform sphere

$$\beta = 1.5\tau \left(1 - \frac{2}{\tau^2} + \left(\frac{2}{\tau} + \frac{2}{\tau^2} \right) \cdot e^{-\tau} \right) \tag{57}$$

[Osterbrock (1974)]

If we guess the level populations in the optically thin radiation case or in the thermal equilibrium case we receive the optical depth and hence the escape probability β. It is very complicated to take both, the radiation and level population into consideration but there are two cases in which this connection disappear:

- when the radiation field in the lines is unimportant for determine the level of population and optical depth
- when the level population (without respect to the radiation field) is in thermal equilibrium. [Rybicki, Lightman (1979)]

CMB can affect the lower level populations of molecules like CO and CS [S. Bruderer (2006)].

1.8.2 The local equilibrium (LTE)

In local thermal equilibrium we assume that the level populations comply with the rules of Boltzmanns equation:

$$\frac{\partial f}{\partial t} + \frac{\partial f}{\partial \vec{x}} \cdot \frac{\partial f}{\partial \vec{p}} \cdot \vec{F} = \frac{\partial f}{\partial t} \tag{58}$$

where $\vec{F}(\vec{x}, t)$ = force field. The term on the right hand side is added to describe the effect of collision between particles. This is the equation of the radiation field. If particels reach the thermal equilibrium through mutual

interaction the time scales for collisions is significantly shorter than that for spontaneous decay: $\frac{1}{C_{21}} \ll \frac{1}{A_{21}}$ or $K_{21}n \gg A_{21}$. In thermal equilibrium the source function becomes the Planck function, but in addition we can simplify the expression for the α_ν because we know the populated levels. In thermal equilibrium and homogeneous medium: $S_\nu = B_\nu(T)$ and

$$\alpha_\nu = \frac{h\nu}{4\pi}\ n_1\ B_{12}\ \left(1 - e^{\frac{-h\nu}{kT}}\right)\ \Phi(\nu) \tag{59}$$

whereas the density of molecules in the lower state can be calculated from the Boltzmann distribution. If we then write our radiative transfer equation in terms of temperature, taking the Rayleigh-Jeans limit, we get:

$$\frac{T_R}{d\tau_\nu} = -T_R + T \tag{60}$$

where $T = T_B$, if the source is homogeneous, optically thick and in thermal equilibrium. The solution of this equation is then:

$$T_R = T\ \left(1 - e^{-\tau_\nu}\right) + T_{\text{brightness}}\ e^{-\tau_\nu} \tag{61}$$

setting $T_R = T_{\text{radiation}} = T_{\text{brightness}}$. The latter is only true if the Rayleigh-Jeans law holds.

2 The programs

2.1 The two-dimensional RATRAN-program: AMC and SKY [Hogerheijde, van der Tak, (2000)]

The two-dimensional RATRAN-program is a formulation of the Monte-Carlo method from the viewpoint of cells rather than photons. The program can be used for optical depths from 10^3 to 10^4. Scattering is neglected. We want to have a numerical method to solve the radiative transfer and molecular excitation in spherically symmetric and cylindrically symmetric source models. M. R. Hogerheijde and F. F. S. van der Tak made therefore use of the accelerated lambda iteration, where the local radiation field and excitation are solved selfconsistently and separated from the overall radiative transfer problem. But they did not discuss the influence of radiative transfer on the source structure [Takahashi et al.,(1983)]; [Ceccarelli et al. (1996)]; [Doty, Neufeld (1997)].

As we already know, the formation of stars occurs in dense condensations within interstellar molecular clouds. The theoretical description is:

$$\rho(r, t = 0) = \frac{a^2}{2\pi G} \cdot r^{-2} \tag{62}$$

where ρ is the density function and a is the isothermal sound speed. At $t = 0$ collapse starts at the centre $r = 0$. After some time t, all regions $r < at$ are collapsing with speed $v(r, t)$ increasing from 0 at $r = at$ to free-fall at $v \propto r^{-0.5}$. The following proportionalities are solutions constructed by Shu (1997).

$$\begin{array}{ll} \text{For } r \ll \text{at:} & \rho \propto r^{-1.5} \\ \text{For } r = \text{at:} & \rho \propto r^{-1} \\ \text{For } r > \text{at:} & \rho \propto r^{-2} \end{array} \tag{63}$$

Collisional and radiative processes can excite molecules and a critical density can be defined as the case, where the two processes are of equal importance (See subsection of Radiative transfer). At low densities radiation dominates, while at higher densities collisions drive the level population to thermodynamic equilibrium. These are physical assumptions taken to program RATRAN. Some other simplifications are made:

For computational purposes, source models are divided into discrete grid cells , each one with a constant density, temperature, molecular abundance, turbulent line width etc. And it is assumed that molecular excitation can be represented by one value for each cell. The velocity can be varied in each cell as well, as the field its the only vector field in the RATRAN code

[Hogerheijde, van der Tak, (2000)]. Therefore we get a finite set of integration paths to construct J_ν, the average intensity, received from all solid angles $d\Omega$ which is defined as:

$$J_\nu = \frac{1}{4\pi} \int I_\nu \cdot d\Omega \tag{64}$$

The radiation field is then the sum of the emission received in each cell from each other cell after propagation through the intervening cells and weighted with the solid angle. The combination of radiative transfer and statistical equilibrium can be written as

$$J_\nu = \Lambda[S_{uk}(J_\nu)]\,. \tag{65}$$

One can think of Λ being a matrix describing how the radiation field in each cell depends on the excitation in all other cells. The upper equation can be solved iteratively. This lambda iteration improves convergence in the presence of significant optical depth. As result we want to get a brightness temperature - velocity spectrum. Since submillimeter frequencies are very high we can approximate the intensity with the Rayleigh-Jeans formula to get a relation between the intensity and the temperature and frequency. Further the Doppler-shift is used to link the frequency with the velocity of the gas particles.

2.1.1 Monte Carlo method [Hogerheijde, van der Tak, (2000)]

One way of solving the upper equation is to directly take the sum over the contribution from all other cells to the radiation field in each single cell. This corresponds to approximate the integral (15) by summation over a random set of directions. So we choose discret values for $d\Omega$ and sum over them. To obtain J_ν, the Monte Carlo method must be adopted.

Scattering is not included in the code, since scattering is not important at the wavelengths of interests, which are smaller than 10 µm. The method is to take randomly generated photon packages, following them as they travel through the source which together approximate the radiation field. We may imagine that every photon in a cell gets its own randomly direction but the same velocity as the others starting their way in the same cell.

Beside estimating J_ν it is also important that non-LTE radiative transfer converge towards the correct solution in a reasonable amount of time. Large optical depth for example can cause that emission passing through an opaque cell will quickly lose all memory of its incident intensity and tend toward the local source function. So the required number of iterations can be found to grow $\propto \tau^2$ which simply is the characteristic of random walk.

With aid of the Approximated Lambda Iteration [Rybicki & Hummer (1991)] it converge much faster in opaque cells, as mentioned before, where the radiation field is close to the local source function. For instance an outflow HCO^+ abundance of 10^{-8} and a inflow HCO^+ abundance of 10^{-10} converges much faster than 10^{-6} and 10^{-8} HCO^+ abundances.

Because the Monte Carlo method estimates J_ν from a randomly chosen set of photon directions, the result has a variance, called σ. This variance depends on the number N of chosen possible directions as $\sigma \propto \frac{1}{\sqrt{N}}$. Since the number of directions is not known in most cases, the variance of a solution is estimated from the largest relative difference between subsequent solutions. It only reflects the noise if random fluctuations dominate the difference.

The Monte Carlo method consists in particular of two stages. First a fixed number of photons will lead to a roughly converged solution. And secondly the number of photons is increased until the noise becomes sufficiently small. In the implementation of Hogerheijde and van der Tak the first stage consists of iterations with a fixed number of directions making up J_ν in each cell. The directions are randomly chosen but in each iteration, the same set of random directions is used by resetting the random number generator for each iteration.

In their code the first stage is considered converged when the noise is ten times smaller than the user-specified level. In the second stage, each iteration uses a different set of random directions to estimate J_ν, thus the random number generator is no longer reset contrary to the first stage. The number of rays in each cell is doubled each iteration, until the noise on the level populations in each cell is below a given value.

2.1.2 Models, Model assumptions and their motivation [Hogerheijde, van der Tak, (2000)]

For the model of Hogerheijde and van der Tak, which are used in this work, continuum radiation fields from dust has been included. If we observe young stellar objects like AFGL 2591, we find flattened structures rather than spherical symmetry of models like that of Shu (1997). These nearly cylindrically symmetric observed structures are presumably caused by magnetic fields and rotation [Hogerheijde et al. (1998)]. Such mechanisms probably have an influence on the accretion behaviour and can give rise to a rotationally supported circumstellar disk. Rotation by Therebey et al. (1984) is treated as small perturbation to the solution of Shu (1997) for a collapsing envelope. The rotation is parameterised by a rotation rate, which gives rise to a centrifugal radius R_c within which the infalling material accretes onto a thin disk. This is what Hogerheijde and van der Tak included in their models and

also that most molecules rapidly freeze out onto dust grains. To make things easier the region within R_c is taken to be empty for calculations.

For molecular observations of protostars the wavelength of the interferometer should be in the millimetre or submillimetre range - with is the case for the observed data of AFGL 2591. Therewith a resolution of about 140 pc can be achieved.

The structure of the circumstellar disk has been modeled according to the effect of warming the disk by thermal radiation of a thin, flared surface layer that intercepts the stellar light. [Chiang and Goldreich (1997)] According to Aikawa and Herbst (1999) freezing out of molecules onto dust grains is one of the most important processes influencing the gas-phase composition in disks, and strongly depends on temperature and density. As closer to the star we are, as higher temperatures can be measured. As one may guess so, away from the midplane densities are lower and the gas-phase abundances are significant. There can also be ultraviolet radiation and X-rays penetrating the upper layer of the disk, which then photodissociate the molecules and increase the abundance of dissociation products like CN. [Aikawa and Herbst (1999)] For the Monte Carlo calculations a grid is used that follows the radial power-law density profile (See following graphics). Young stellar objects with

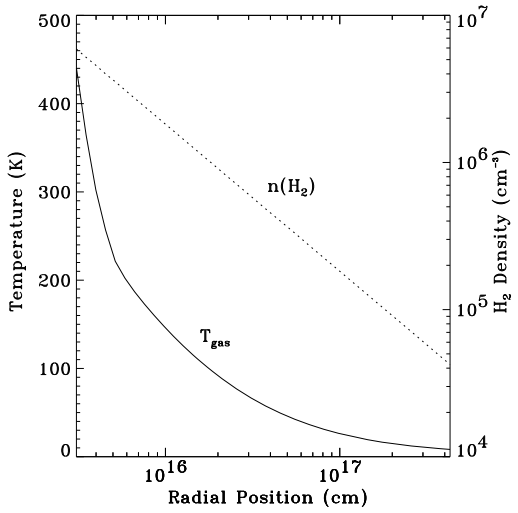

Figure 1: Model data by P. Stäuber: The power law density distribution is adopted from the model of van der Tak. et al. (1999). The gas temperature profile is calculated by Doty et al. (2002)

luminosities of $10^4 - 10^5 L_\odot$ heat significant parts of their envelopes to several hundred Kelvin. This causes a shift in the peak of the Planck function to the wavelengths of the vibrational transitions of many molecules. On the other

hand, stars of lower mass and luminosity only heat small regions to a few hundred Kelvin, and the impact on the excitation is much smaller. An often made approximation is that it's assumed: $T_{gas} = T_{\rm dust}$ which holds only for high density regions.

The infrared pumping by dust can be observed in the shells around evolved stars and is essential to understand the rotational line emission. Dust emits its radiation particullary in the infrared, after having absorbed radiation from the star. This is what is so called infrared pumping.

2.2 The RATRAN code - AMC and SKY written by Hogerheijde et al.

The first step is to run the Monte Carlo simulation solving the radiative transfer and molecular excitation. With this solution the emission that would be observed from the source, above the atmosphere and assuming a perfect spatial and velocity resolution, will be calculated by the second step of the code. Therefore we had to define a source distance and for our cylindrically symmetric two-dimensional model also an inclination, which defines the line of sight.

The output of this program is then in a MIRIAD code (Multicannel Image Reconstruction, Image Analysis, and Display. [Sault et al. (1995)]) To converse this to a FITS format file a program written by P. Stäuber has been used.

The Monte Carlo part of the code can be described in the following steps:

1. **In a first stage** the program reads the keywords, like the signal-to-noise ratio (SNR) on the level populations and the initial number of photons in each cell. Furthermore it creates pointers to the source model, add the systematic velocity field, the description of the dust emissivity, the molecular energy levels and the collisional rate coefficients. The last two are given by Schöier et al. (2004).
2. Each ray in a cell, all rays being randomly distributed over the cell, starts with a random direction, at a random frequency. In each iteration the same series of random numbers is used that no random fluctuations are caused in the overall radiation field.
3. Further the distance ds from the ray's origin to the nearest boundary of the cell along its randomly chosen direction is calculated. The incoming radiation along the ray is given from the integration of equation (17) from cell edge to cell edge. The cosmic microwave background is used as a boundary condition. The only two values which may change during

passing the cell are the direction and the velocity, depending on the line profile function $\Phi(\nu)$.

4. With this set of values for ds, $\Phi(\nu)$ and I_0, for each ray the code calculate the radiation field J_ν in the cell.
5. Now this steps of the code will be repeated until the largest relative fractional difference between the populations in all cells of three subsequent solutions is ten times better than finally required.
6. **The second stage** of the code proceeds along similar lines, but with a different set of random numbers in each iteration. Another difference is, that each time the maximum fractional error in the populations in a cell exceeds the requested accuracy, the number of rays in that cell is doubled.

The second part of the code calculates the emission distribution on the sky for a given source distance and inclination by ray tracing. The output from the first part of the program (Monte Carlo code) is the input for this ray-tracing code. Further details can be found in the paper [Hogerheijde, van der Tak, (2000)].

2.2.1 The AMC input file - generated by a Velocity Model program

The input file for AMC consists of several rows of values that are constructed from different models. In two dimensional case, which will actually be the main part of this work, the parameters of the input file are (sorted by row):

r_a inner coordinate of the cell in r-direction [m]

r_b outer coordinate of the cell in r-direction [m]

z_a inner coordinate of the cell in z-direction [m]

z_b outer coordinate of the cell in z-direction [m]

nh abundance of H_2 [particles per cm^{-3}]

nm abundance of the molecules we are interested in [particles per cm^{-3}]

tk temperature of the gas (in our case of the protostar AFGL 2591) [Kelvin]

db line width $[\frac{\mathrm{km}}{\mathrm{s}}]$

v_r velocity of the molecules in r direction $[\frac{\mathrm{km}}{\mathrm{s}}]$

v_z velocity of the molecules in z direction $[\frac{\text{km}}{\text{s}}]$

v_a velocity of the molecules in the azimuthal direction $[\frac{\text{km}}{\text{s}}]$

td temperature of the dust (in our case of the protostar AFGL 2591) [Kelvin]

The models used for each of these parameters: (Also see grafics (1))

- For r_a, r_b, z_a and z_b we constructed cells, that are equally distributed in space in the logarithmic scale in the two dimensional space. The cell in the middle, where the star is, is much bigger than all other cells, since there is no observational data or models available for the most inner region. We set the inner minimal radius, which then correspond to r_a and z_a of the most inner cell, to be $3 \cdot 10^{13}$ m. The maximal radius of the considered region is chosen to be $1.103 \cdot 10^{15}$ m m.

- To find out the abundance of H_2 (nh), we adopted the model from Jorgensen, Schöier and van Dishoeck (2003) or also van der Tak et al. (1999), where
$$nh = n_0 \cdot (\frac{\sqrt{(x^2 + y^2)}}{r_0})^{-p} \tag{66}$$
and x and y are the coordinates of the centre of each cell. The constants $n_0 = 4.234 \cdot 10^{15} m$ and $r_0 = 4.234 \cdot 10^4 cm^{-3}$ are calculated by Stäuber et al. Assuming the model of $nh = \rho \propto r^{-p}$ and a static envelope density distribution
[Jorgensen, Schöier and van Dishoeck (2003)] it results:
$$r^{2-p-q} = \text{const.} \Leftrightarrow q = 2 - p \tag{67}$$
where p is observed to be one for AFGL 2591, and therefore $q = 1$. One can see, that in a logarithmic plot the density distribution will be linear while the energy distribution and accordingly the temperature distribution is more likely an exponential function, which drops off rather fast. (Also see graphics (1)) In a second step we made a difference between out- and inflowing gas of the protostar, by setting
$$\frac{n^{\text{in}}(H_2)}{10} = n^{\text{out}}(H_2) \tag{68}$$

- To fix nm we first considered the ratio of nm/nh to be $1 \cdot 10^{-10}$ for the two dimensional model to get the temperature spectra of different molecules like HCO^+ or CS. But then a inflow and a outflow regional density ratio nm/nh for the gas is set separately. A half cone of 15°

for the outflow and one of 75° for the inflow gas region is defined for a quarter of a sphere. As it is all symmetric, an integration over the space make the cones complete (to a 30° and 150° cone for the outflow and the inflow region respectively). This values are calculated by [van der Tak, van Dishoeck, Evans II, Bakker and Blake (1999)]. Each value for this ratio can be seen in the comments for each diagram in the appendix. In the 150° angle, which is the half cone for the inflow region, it is assumed that the density ratio is always higher or equal to the ratio in the outflow.

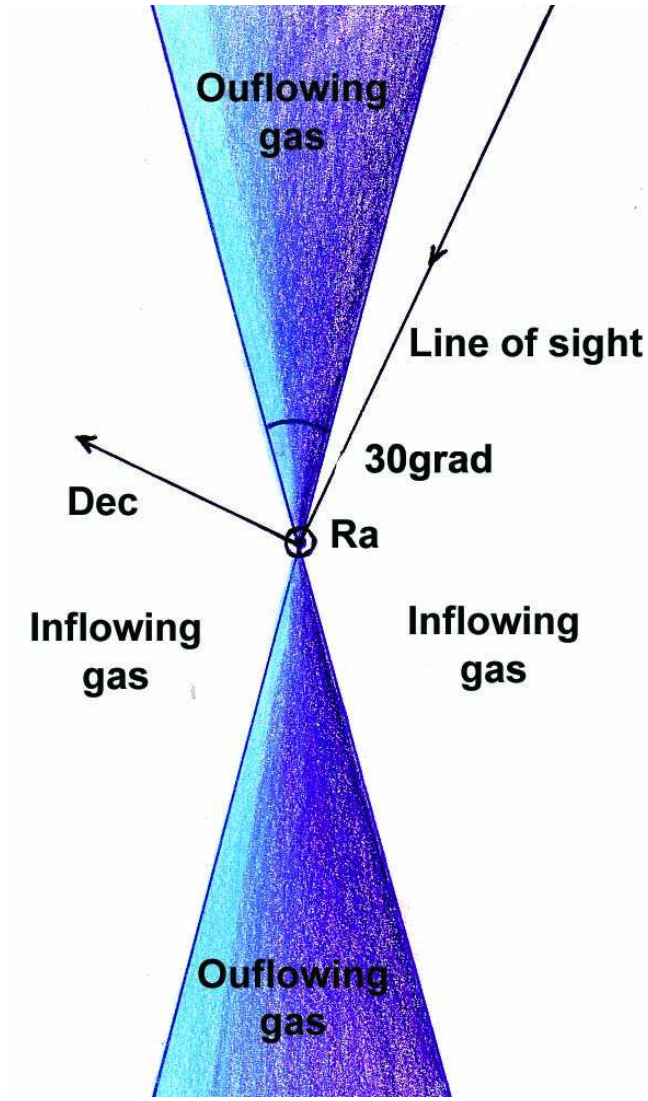

Figure 2: Model of in- and outflow gas region

- The temperature of the gas *tk* and the one of the dust *td* are set to be equal, as mentioned before (equation (30)). The models for these values in the input file for AMC are complicated and therefore we used a interpolation of the one dimensional model from P. Stäuber (2005) to get reasonable temperatures for all possible cell within the maximal radius. Further we differentiated between the two gas regions outflow and inflow. It is assumed that:

$$T^{\text{out}} = 2 \cdot T^{\text{in}} \tag{69}$$

- *db* = FWHM · factor of the gaussian function normalisation (being 0.6). In a first step the line width *db* is chosen to be 1.6 as it was in the one dimensional model and as typical widths are around $1\,\frac{\text{km}}{\text{s}}$ (FWHM) [Jorgensen, Schöier and van Dishoeck (2003)]. But then we did a second effort by using the formula:

$$db = \sqrt{\frac{k_B T_{\text{gas}}}{m_{\text{molecule}}}} \tag{70}$$

  where k_B is the Boltzmann-constant. The main molecule which was considered for this work was HCO^+.

  Furthermore we multiplied *db* by a factor to adjust it to the Gaussian fits to observed submillimeter emission lines from [van der Tak, van Dishoeck, Evans II, Bakker and Blake (1999)], which states that the transition $4 \rightarrow 3$ of HCO^+ should have a FWHM of $4.56\,\frac{\text{km}}{\text{s}}$.

- The velocity v_a is set to zero in a first approach. As we have already seen most of the observed spectral lines are simple Gaussians. But there is a broadening due to systematic or turbulent motions required to get the exact line profiles. In our case the velocity field v_r and v_z for the inflowing region has been received by interpolating the velocity distribution of the one dimensional model written by P. Stäuber et al. The radial component v_R is therefore splitted into two vectors; v_r and v_z according to the new coordinate in the two dimensional system. That is for the inflowing gas region. The outflowing region has another velocity behaviour. The second model applied, is based on observational findings. The outflow is assume to be radially constant. Which means that we set $v_r = 4\,\frac{\text{km}}{\text{s}}$ and then separate it into two components: v_r and v_z as we did in the inflow region. For the Kepler-model see the separate chapter.

2.2.2 Line.mir written by P. Stäuber

This program has the aim to convolve the model data with a beam of the size of the observable width and intensity of the specific telescope. Therefore the scale and FWHM is needed to run the program. For AFGL 2591 P. Stäuber chose for the transition $4 \rightarrow 3$ of HCO^+ FWHM = 20 and scale $= 2.21 \cdot 10^{-5}$ and for the transition $5 \rightarrow 4$ of HCO^+ he used FWHM = 14 and scale $= 4.50 \cdot 10^{-5}$. What is returned by the program is a fits-file instead of the entered sky-file.

2.2.3 Cf.class by P. Stäuber

This program reads a fits-input-file and converts it to a bur-type file written in the programming language of class.

2.2.4 Show.class by P. Stäuber

Finally show.class converts the output-file from cf.class to an eps-graphic.

3 Results

The goal of this assignment was to fit the theoretical models to the observed data which was taken last summer(2005) with the Submillimeter Array Telescope (SMA) on top of Mauna Kea at an altitude of 4092 m in Hawaii. This Submillimeter-Interferometer has eight antennas each with a diameter of six meters. They are operated by the Smithsonian Astrophysical Observatory at Harvard University in Cambridge. 2002.

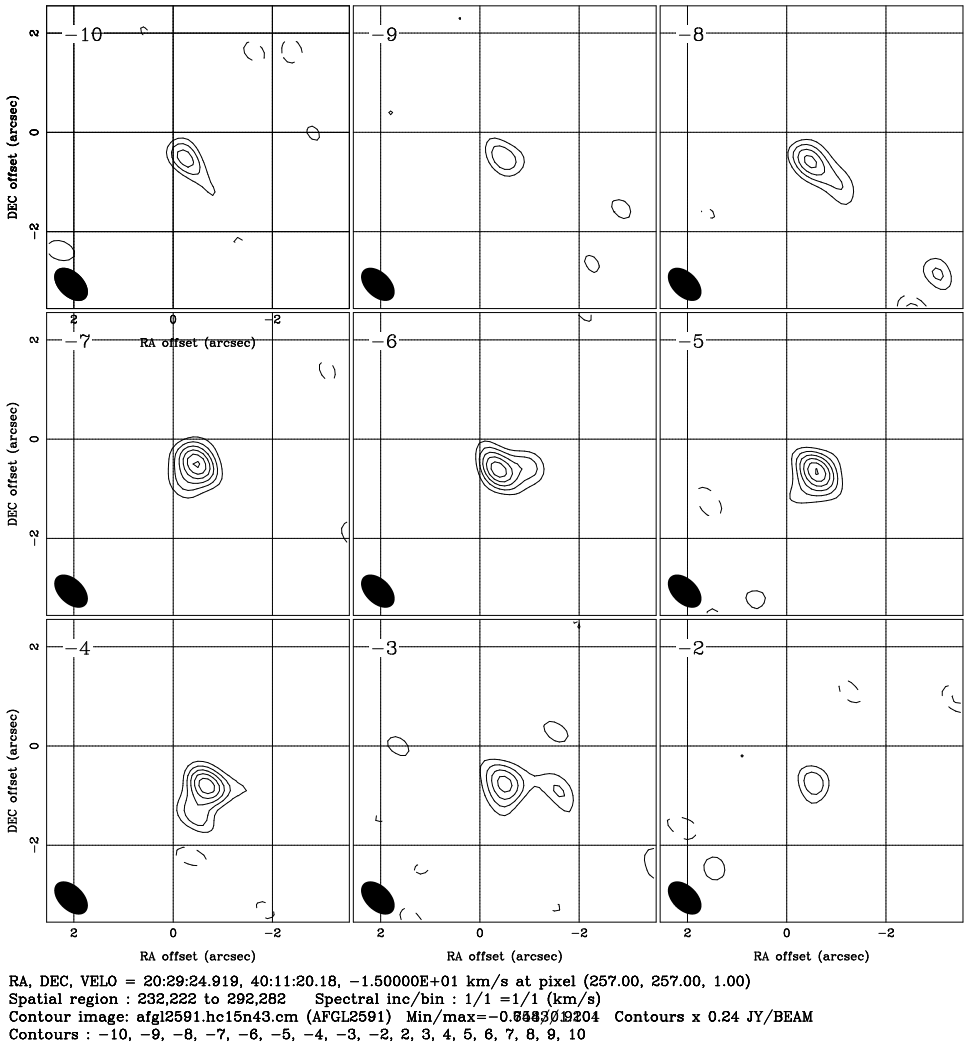

Figure 3: Observational data of AFGL 2591, inclination angle = 25° and outflow angle is approximately 30°

3.1 Brightness temperature spectra and asymmetric lines [Stahler, Palla (2004)]

The problem of protostars is that they are still buried in the dense cores that spawn them. The surrounding dust and gas absorbs much radiation from the accretion shock and the stellar interior. We are able to find out about the properties of grains in the dust, because of the reemitted energy of the photosphere. To find protostars one compares the emitted fluxes from known sources with the results one expects in an infalling environment. First a quantitative model has to be constructed, which is a rather hard work. All models have some things in common: First a density, a temperature and an inflow velocity that rises toward the star. A second generic feature is that the interior region should be of relatively low optical thickness.

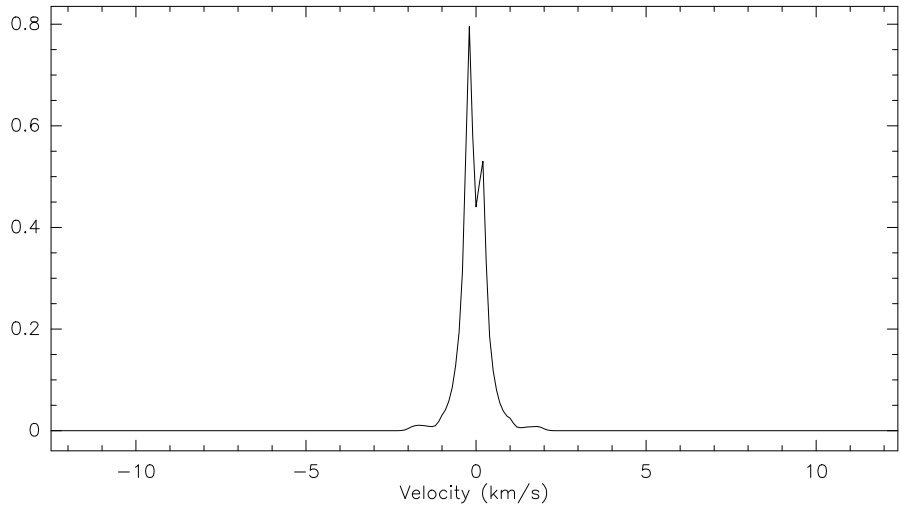

Figure 4: velocity spectrum

A flat-topped appearance like in fig. (9) can be associated with saturation broadening of optically thick profiles. Also a common feature of optically thick lines is if the HCO^+ profile shows a pronounced dip close to the line centre. This central depression reveals the presence of relatively cold, foreground gas that absorbs photons from warmer material behind it. It is called foreground gas because it does not participate in the bulk motion, but is static. This gas is the reason for this dip at the line centre. The temperature rises as we climb deeper into the cloud, because of irradiation by the embedded star.

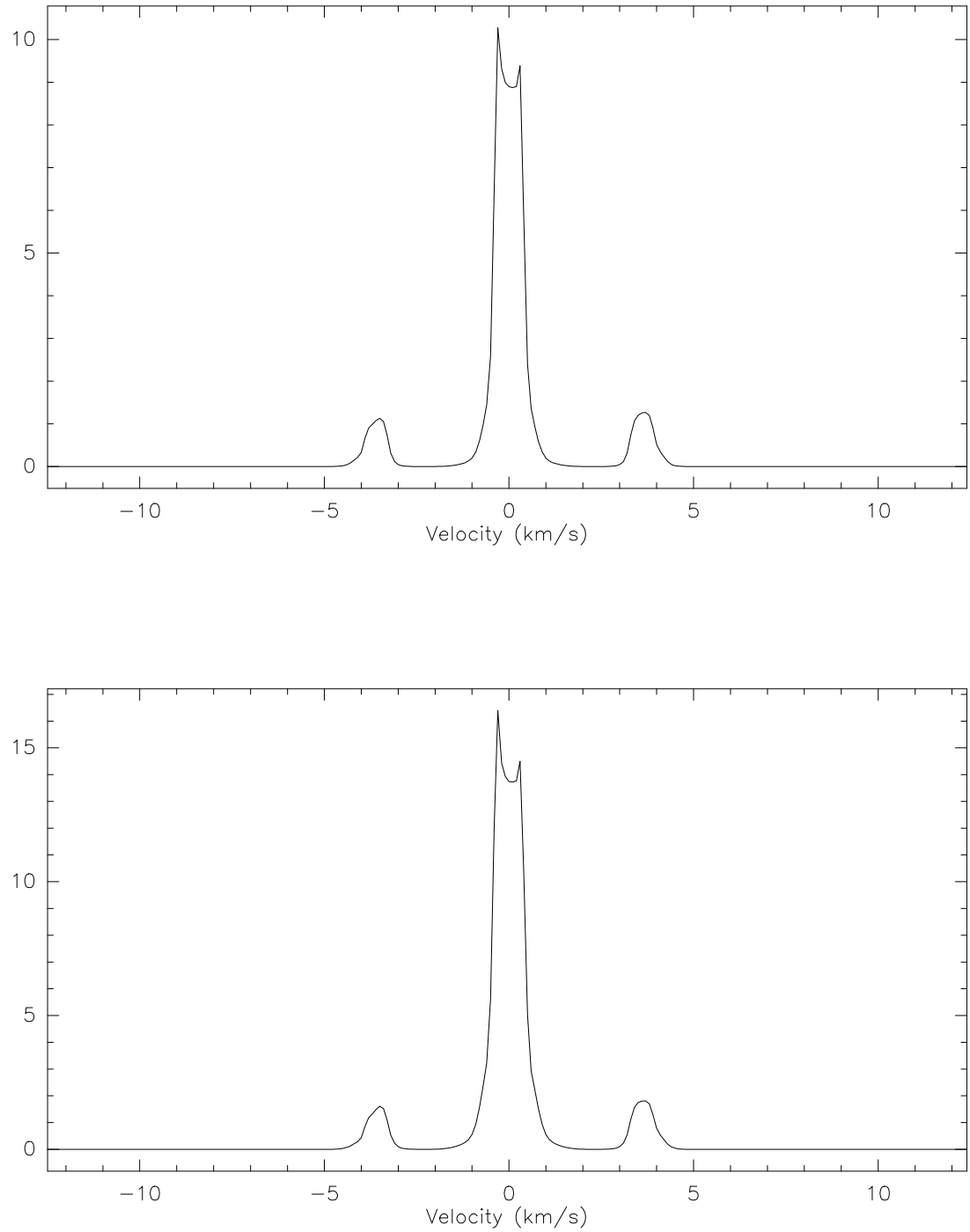

Figure 5: Velocity spectrum of the velocity model with a in- and outflow region, transition $4 \rightarrow 3$ and $5 \rightarrow 4$

There is also a speciality in the asymmetry of the optically thick profile, with the redshift side depressed relative to the blue (fig. (6)). One possible interpretation is that the bulk motion in these cases is actually collapsing onto the star.

Two peaks in the line centre are only because particles move and are not static. That is the reason for particles to have a Doppler shift in their spectra since all particles flying towards the observer are blueshifted and the others are redshifted, which means to a negative or a positive velocity respectively. That is why in the temperature spectrum all blueshifted particles have negative and the redshifted have positive velocities.

Infalling gas from the far side (region 4) emits blueshifted photons, because it is approaching the observer as inflowing gas - if the inclination of the observer is still taken to be 25°. (See graphics (6)) Conversely the outer side of the cloud - an infalling region as well - contributes to the redshifted part of the profile. Blueshifted photons originate closer to the cloud's centre where the temperature is higher. Consequently the brightness temperature is elevated in the profile for blueshifted particles. Most of the redshifted photons are emitted from the outer region of lower temperature. The feature of asymmetric lines is a typical sign for a beginning collapse.

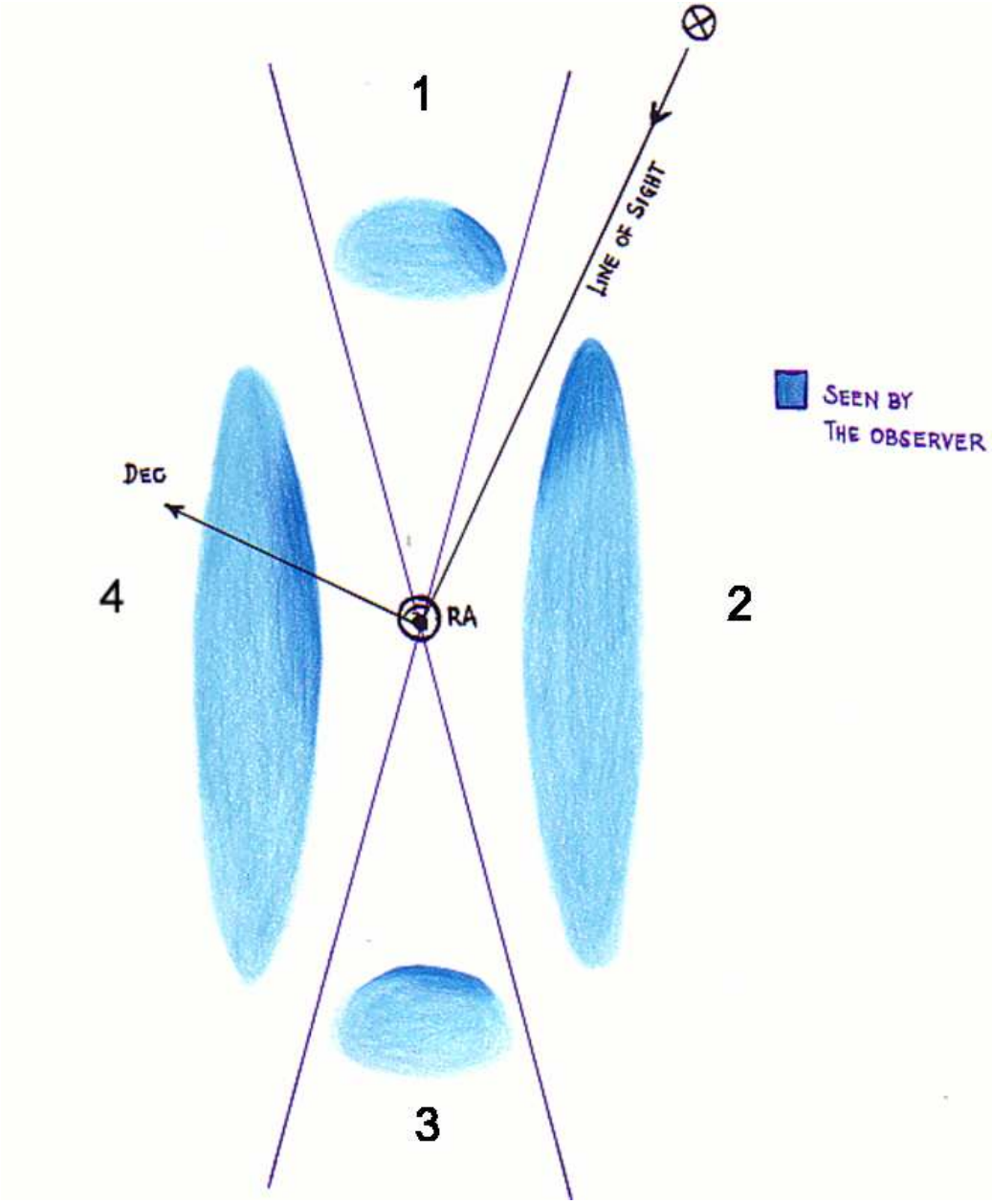

Figure 6: Four regions of the protostar

3.2 Interpretations of Velocity Model - Results

Different models were developed and in this section the results are summarised. It has to be pointed out, that this assignment topic is still a topic of today's research programs and therefore many effects are not understood and interpreted yet. This assignment is partially a try to have some new ideas verbalised.

The interpretation of temperature spectra of different molecules of the dust cloud around a protostar: Taking the HCO^+ molecule which originates from the following reaction, our calculations converged quite fast due to the optically thin medium. Additionally we set the abundances $\frac{nm}{nh}$ for the inflow region as well as for the outflow region to $\frac{nm}{nh} = 10^{-10}$. The velocities of the molecules are firstly taken to be zero everywhere before creating a velocity model. That is the reason why the plot shows a Gaussian shaped curve. The scale on the y-axis is the temperature in units of Kelvin. The reactions which produces HCO^+ are:

$$H_2 + \gamma \rightarrow H_2^+ + e^- \tag{71}$$

$$H_2^+ + H_2 \rightarrow H_3^+ + H \tag{72}$$

$$H_3^+ + CO \rightarrow HCO^+ + H_2 \tag{73}$$

It is interesting when comparing the two transitions $4 \rightarrow 3$ and $5 \rightarrow 4$ (fig. (7) and fig. (8)) that the brightness temperature curve for the higher transition is little higher eventhough one knows that less photons are on the fifth energy level than on the fourth. The proper explanation is that photons with a higher energy are emitted in the more inner region of the protostar, where the energy is high and therefore particles absorb much more energy and thus the global brightness temperature in the diagram rises.

It is also interesting that the one dimensional model (fig. (8)), which should be equal to the upper diagram (since we doesn't make any differences in out and -inflow) isn't exactly equal in the height of the peak in the two dimensional model. The reason must be the different amount of cells taken in the two models.

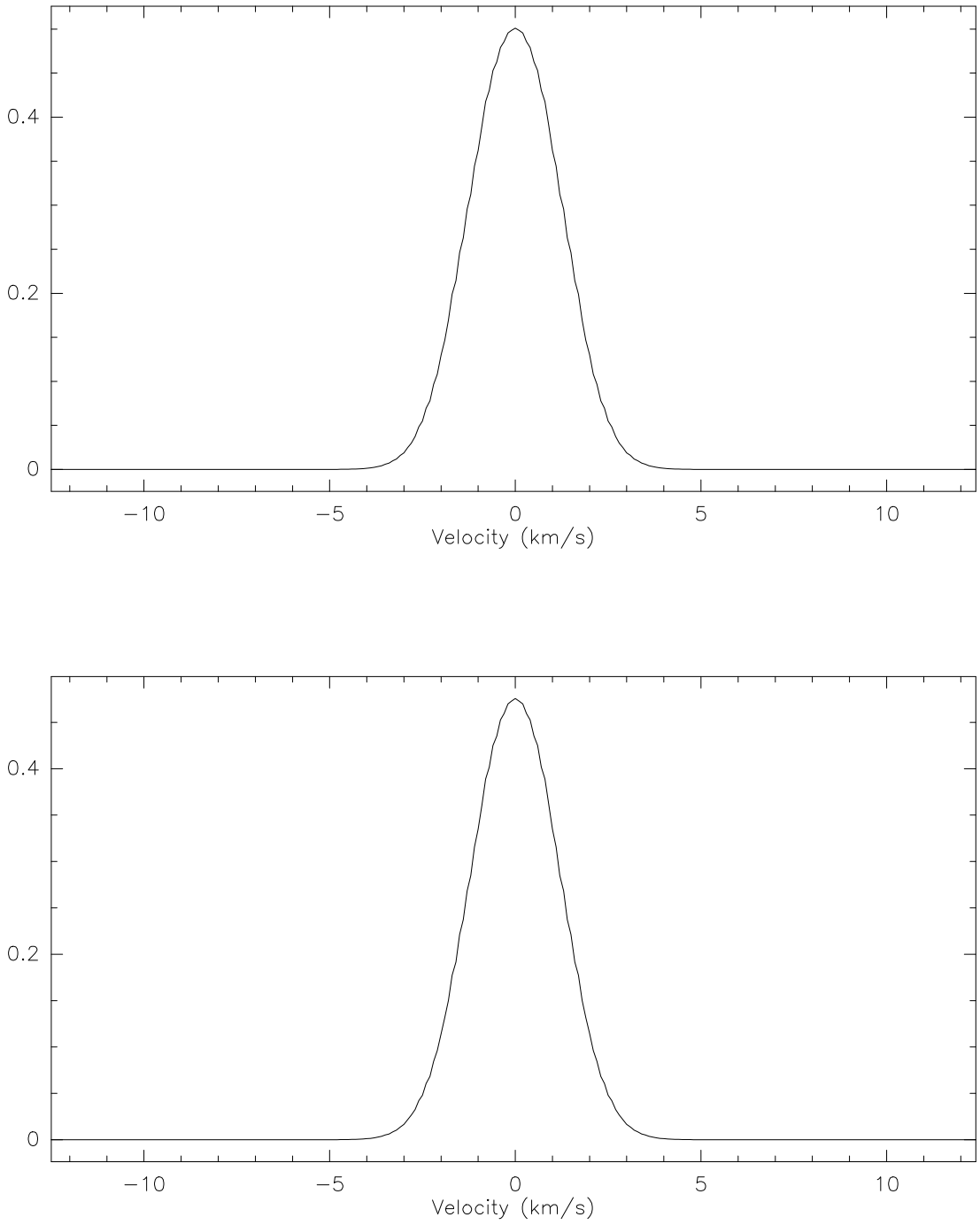

Figure 7: Temperature spectrum of the non-velocity model

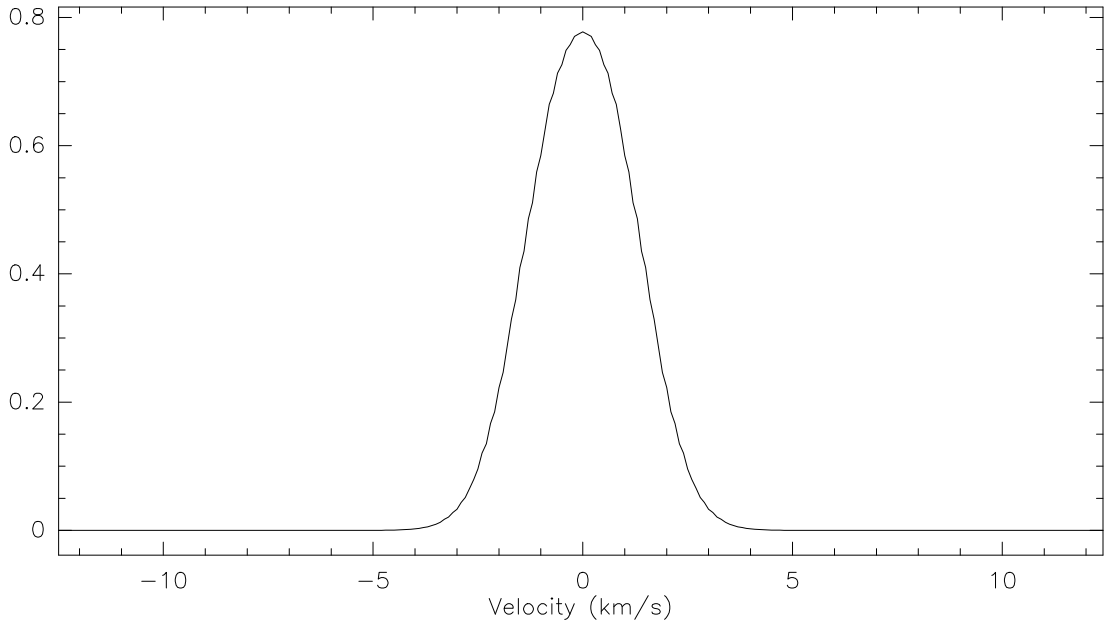

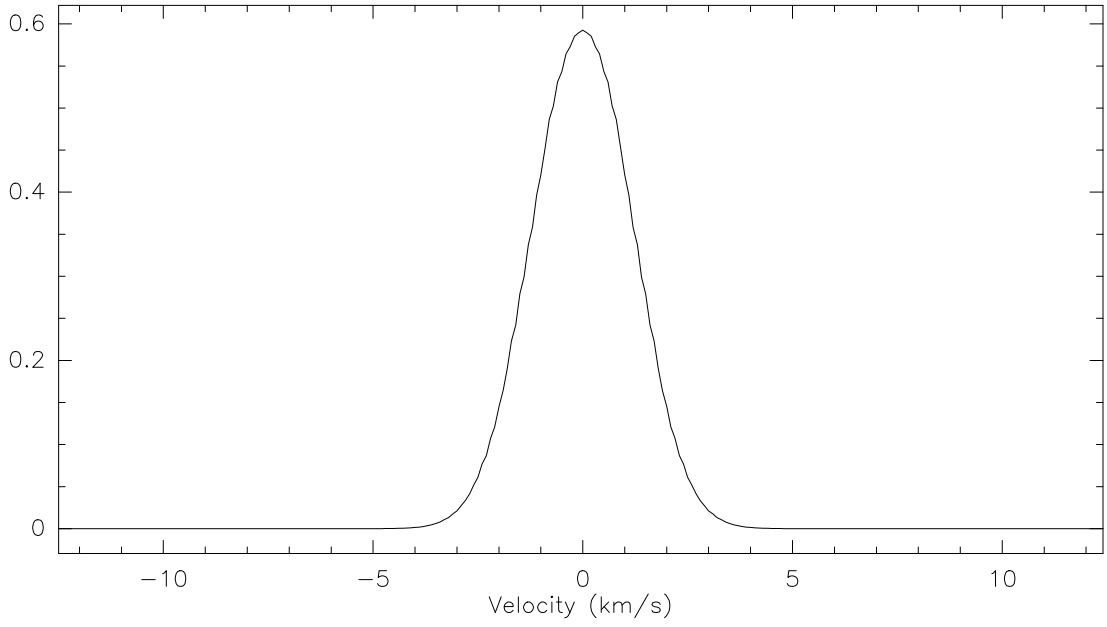

Figure 8: Temperature spectrum of the non-velocity model

In graphics (9) the CS molecule is used for our calculations. The abundances are fixed at $\frac{nm}{nh} = 10^{-10}$ for both, the inflow and the outflow region of the gas. It is obvious that it is optically thick because photons are absorbed by the gas and dust in the profile centre line. Due to this strong absorbance higher energetic photons (from the transition $8 \rightarrow 7$) emitted in the inner region loose more energy on their way to the observer on earth so their peaks reaches a smaller temperature level compared to the transition $6 \rightarrow 5$ which occurs in colder regions where the gas does not absorb as much as in the hotter inner region where the gas is much denser. But as the photons of the $8 \rightarrow 7$ transition have more energy and therefore a higher chance to escape the dust, the plot appears to be less optically thick than the $6 \rightarrow 5$ transition plot; less optically thick meaning the sphere around the centre of the star inside which all photons are completely absorbed by the gas particles, has a smaller radius.

As we know, the molecules do not have an average velocity of $0\,\frac{\mathrm{km}}{\mathrm{sec}}$, the IDL-program to generate the input-file for the RATRAN program, needs to be adjusted for the Velocity-Model. (See chapter: The AMC input file - generated by a Velocity Model progam)

The next question we wanted to have an answer to is: What changes in a spectrum if the outflowing gas is taken to be $4\,\frac{\mathrm{km}}{\mathrm{s}}$ instead setting the radial velocity to zero? Therefore the two fig. (10) can be compared. The result is that the two peaks which are Doppler shifted are consequences of the outflowing gas. The inflow has an influence on the two centred peak around velocity zero, as can be seen in fig. (11). This is logical since the left hand peak is higher then the right one. See previous chapter: Asymmetric lines where this is all explained properly.

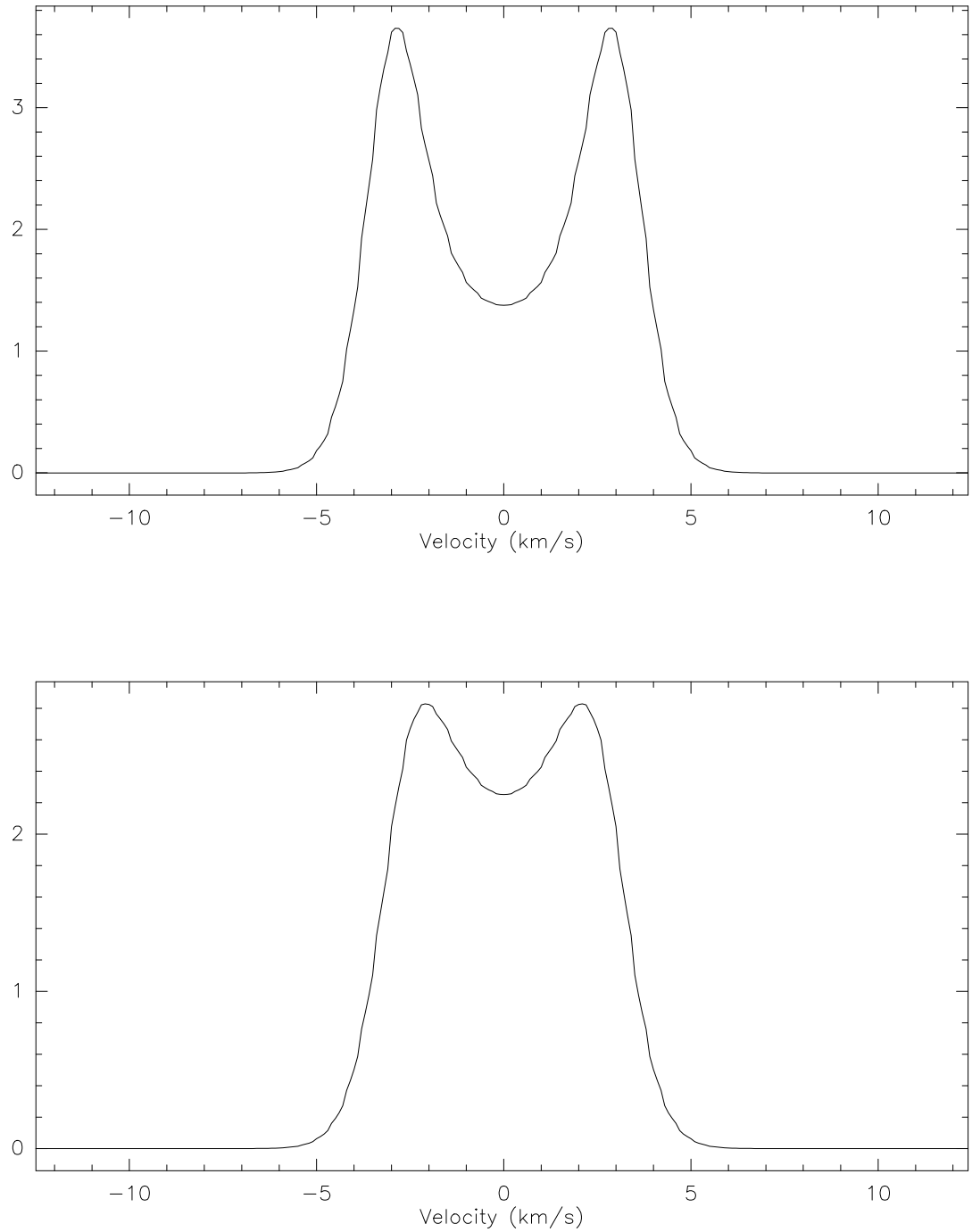

Figure 9: Temperature spectrum of the non-velocity model, top:6 $\rightarrow$ 5 , bottom: 8 $\rightarrow$ 7

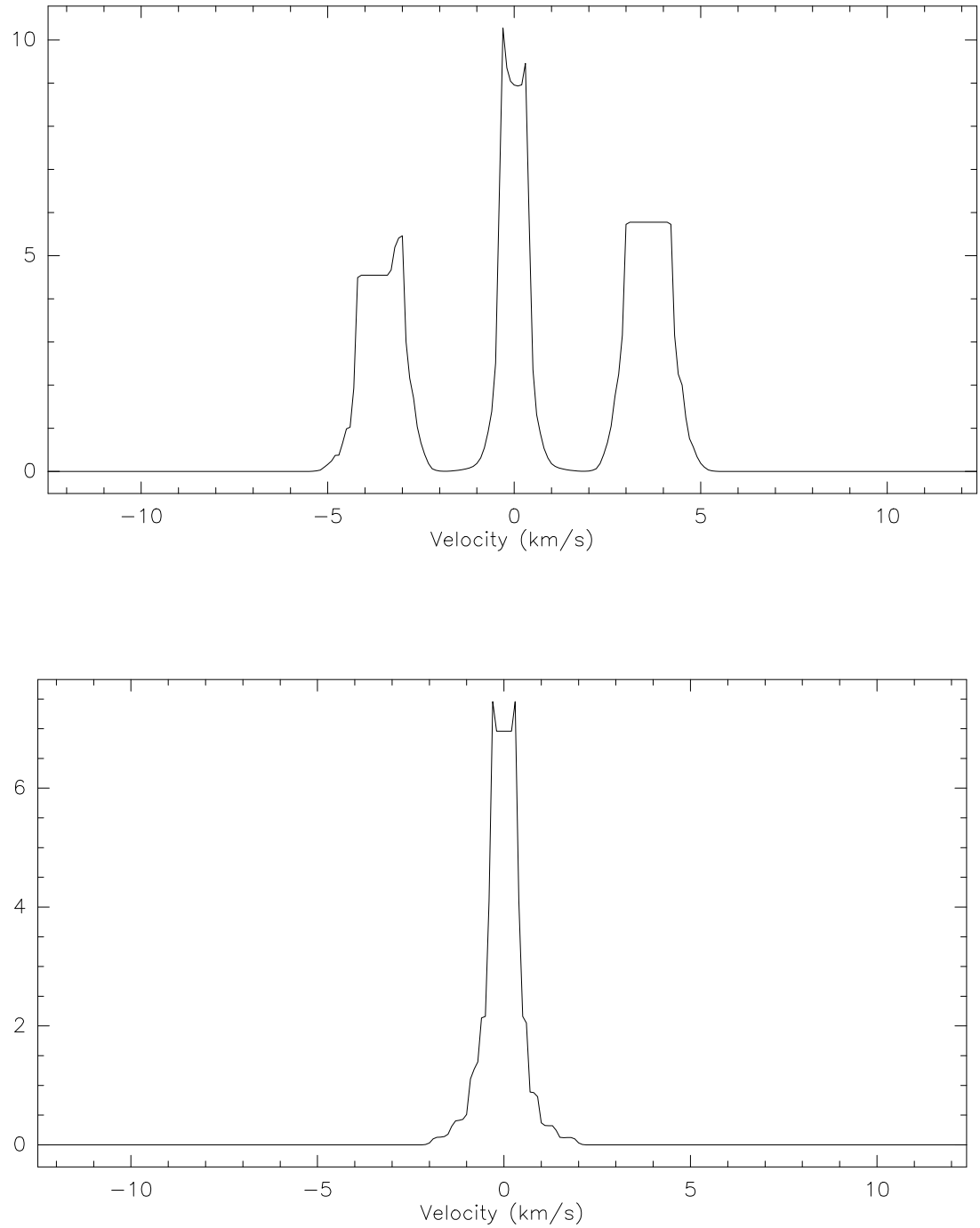

Figure 10: Temperature spectrum of the Velocity model (At the top: with outflow $v = 4\,\frac{\mathrm{km}}{\mathrm{s}}$, at the bottom: without outflow v= $0\,\frac{\mathrm{km}}{\mathrm{s}}$)

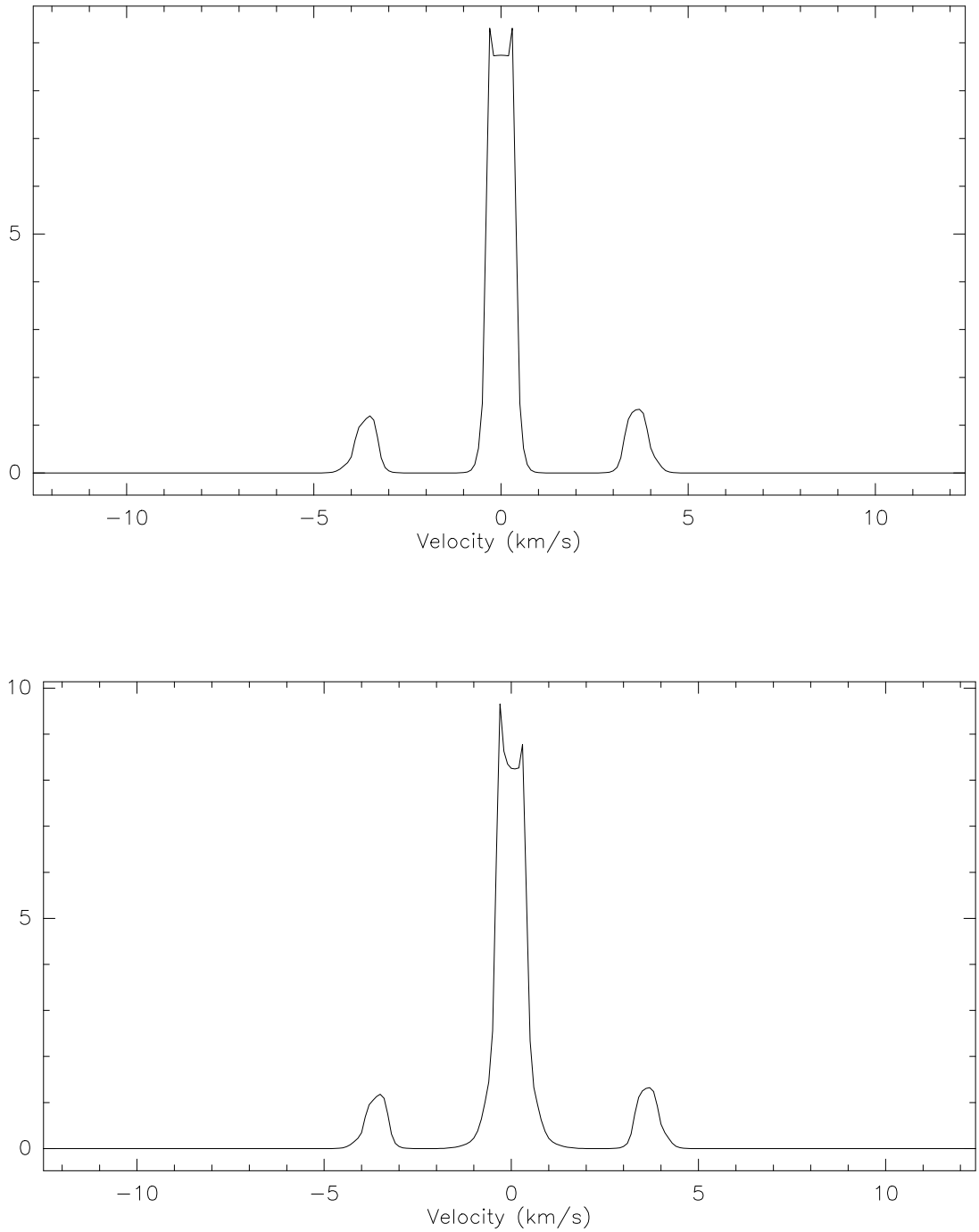

Figure 11: Temperature spectrum of the Kepler-Rotation model, without (at the top) and with (at the bottom) inflowing gas

The db is the one parameter which can be shifted by multiplying with the ratio

$$\frac{FWHM_{\text{new}}}{FWHM_{\text{old}}} \tag{74}$$

to get the desired value and thus the required width of the profile.

The inclination defines the direction of the line of sight. If nothing else is entered in the program's input-file our view goes directly into the outflow region of the protostar. The following directions we calculated the radiative transport for:

- $0°$ = line of sight directly into outflow region
- $15°$ = in the transition between in- and outflow
- $25°$ = in the inflow region
- $30°$ = in the inflow region
- $45°$ = in the inflow region
- $60°$ = deeply in the inflow region

But what can we read out these numerous plots (fig. (12) - (17))?

1. While we keep the same molecule, molecular energy level transition and molecular density ratio, the height of the peak should not and in fact doesn't vary very much.

2. We have already seen, that the two small peaks in the line centre are caused by the inflow. If we change our view of observation from the outflow to the inflow region, these small peaks disappear or at least decrease. We presume that the reason is that we now observe the photons emitted from the high temperature region though a partially cold gas region, which absorbs many photons.

3. We fixed the outflow velocity to $4\,\frac{\text{km}}{\text{s}}$. By observing directly in the line of the outflow, we have therefore two strong peaks at velocity $4\,\frac{\text{km}}{\text{s}}$. But if we change our line of sight by carrying the inclination to the inflow region, the profile of these two outflow peaks get broader and flatter. It also shifts the maximum to a lower velocity which obviously is a component of the outflowing radial $4\,\frac{\text{km}}{\text{s}}$ vector.

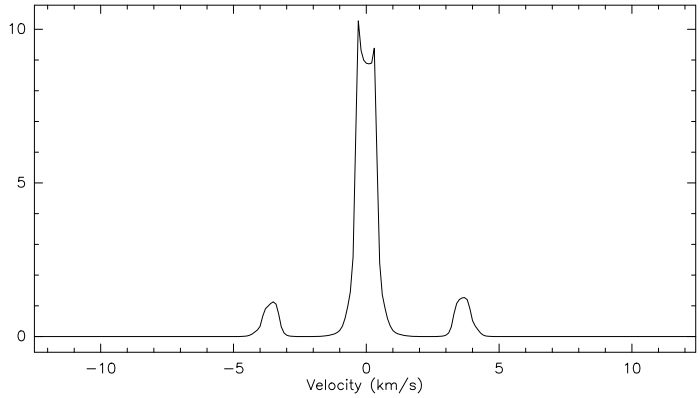

Figure 12: Temperature spectrum of the Velocity model with inclination: 0°

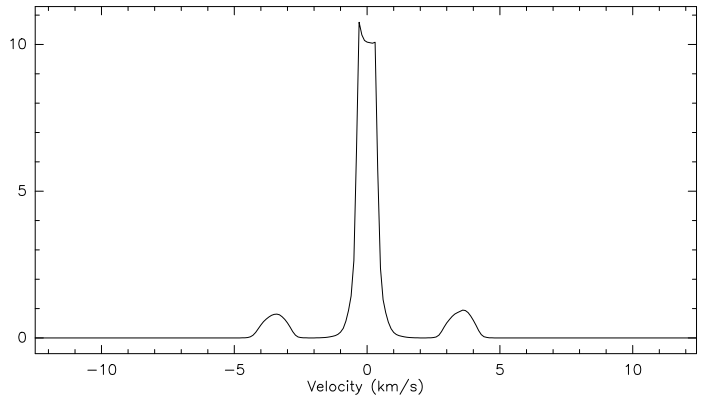

Figure 13: Temperature spectrum of the Velocity model with inclination: 15°

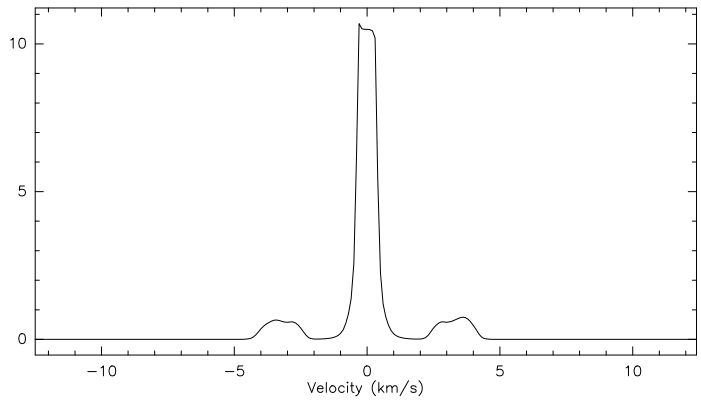

Figure 14: Temperature spectrum of the Velocity model with inclination: 25°

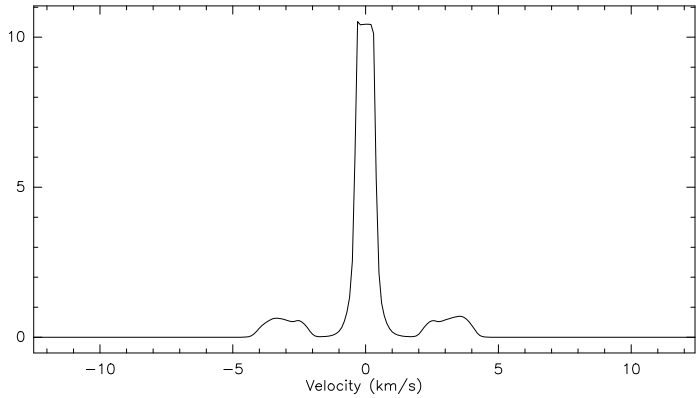

Figure 15: Temperature spectrum of the Velocity model with inclination: 30°

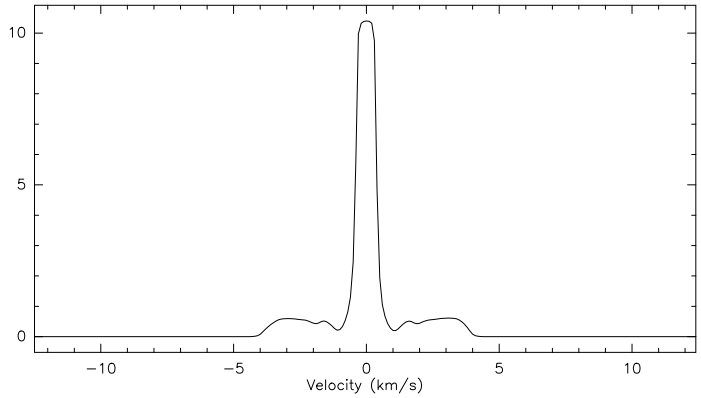

Figure 16: Temperature spectrum of the Velocity model with inclination: 45°

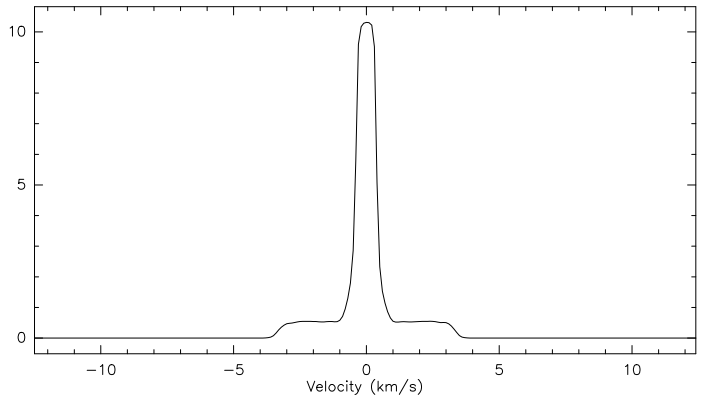

Figure 17: Temperature spectrum of the Velocity model with inclination: 60°

In the next step maps are made of different regions of the temperature-velocity spectrum. A map is a representation of contour lines of particle detections with the same intensity and also temperature, since these quantities are proportional to each other. The three different velocity intervals taken for fig. (18), (19) and (20) are:

$$I_1 = [-5, -2]$$
$$I_2 = [-2, +2]$$
$$I_3 = [+2, +5]$$

The inclination is zero degree, thus the maps have to be more or less symmetric because the particles move only outwards and are not rotating in a Kepler-rotation way.

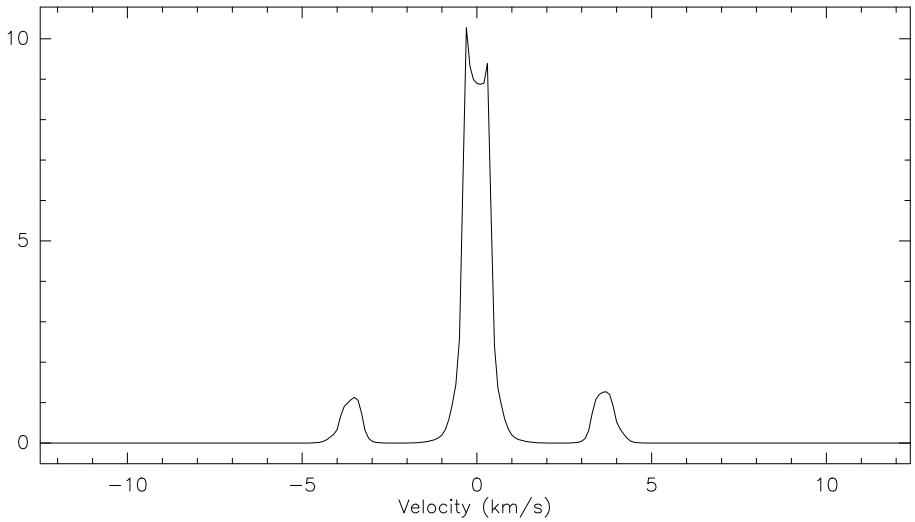

Figure 18: Temperature spectrum of the Velocity model

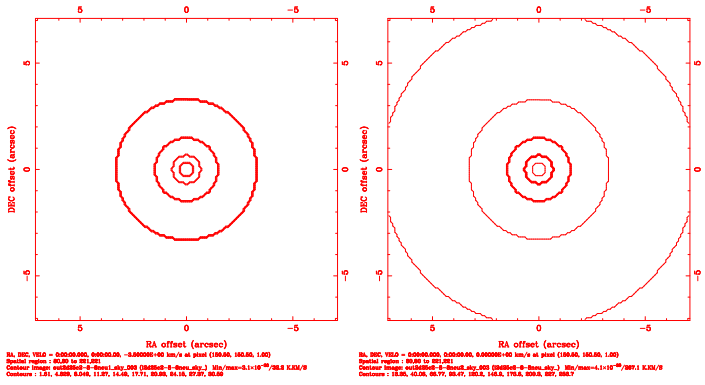

Figure 19: Intensity contour lines of the Velocity model with average velocity $= -3.5\,\frac{\text{km}}{\text{s}}$ and Intensity contour lines of the Velocity model with average velocity $= 0\,\frac{\text{km}}{\text{s}}$

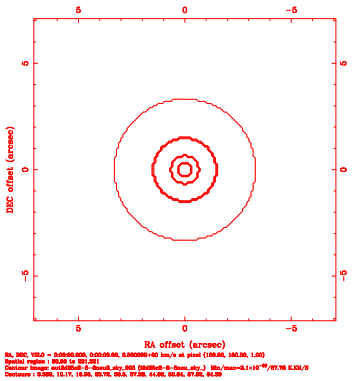

Figure 20: Intensity contour lines of the Velocity model with average velocity $= +3.5\,\frac{\text{km}}{\text{s}}$

The procedure to get maps that are similar to the observational data is as follows: In fig. (21) *db* has to be multiplied by a factor that we roughly receive a FWHM of 4.56, proposed by [van der Tak, van Dishoeck, Evans II, Bakker and Blake (1999)]. In order to get best fitting results we set an inclination of 25°, which may be estimated from the pictures of AFGL 2591. Van der Tak et al. deduced this feature from the observations. To make sure that this spectrum is optically thin, abundances in the inflow region of 10^{-10} and in the outflow region of 10^{-8} are taken. In exactly the same way as we did convolve the temperature spectrum with our beam - determined by the telescope features, we convolved our maps with a beam of FWHM = 0.6. This restrains the diagram such that it becomes possible to compare observational data with the theoretical model data set. (See fig. (2))

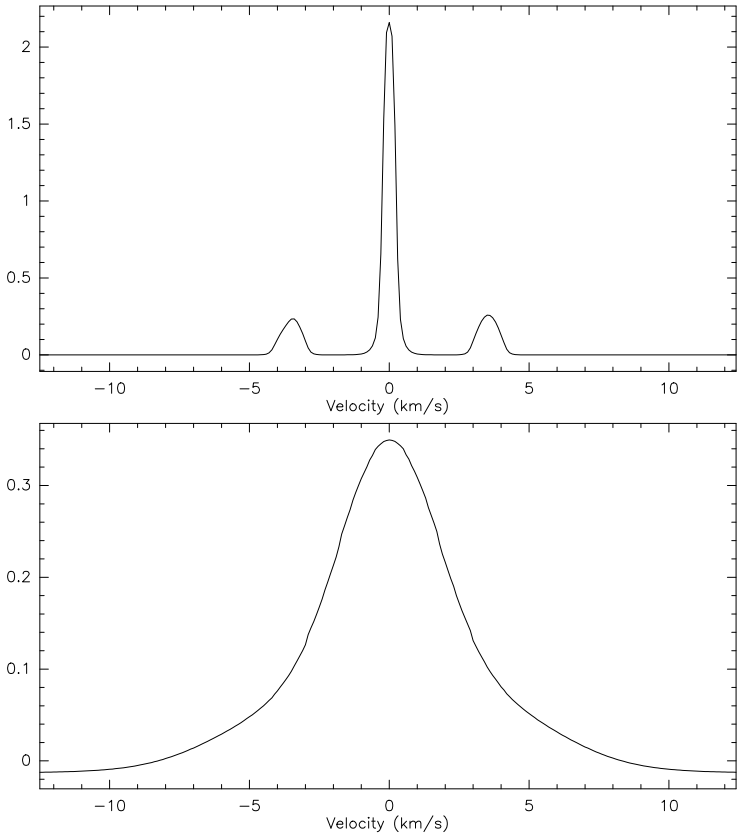

Figure 21: Temperature spectrum of the velocity model without db adjustment and with db adjustment

3.3 Interpretation of the velocity model profiles for optically thin and optically thick spectra and its maps

Maps also do give more informations about the position of a certain intensity. While in the brightness temperature spectrum plot the intensity is a integral over a given velocity interval strictly speaking a number, the contour lines in a map are lines of equal intensity distributed in a defined spatial region of the sky. Hence a map contains additional information.

For an inclination of the observer of 25° we can interprete the velocity-model maps as illustrated in the following graphic:

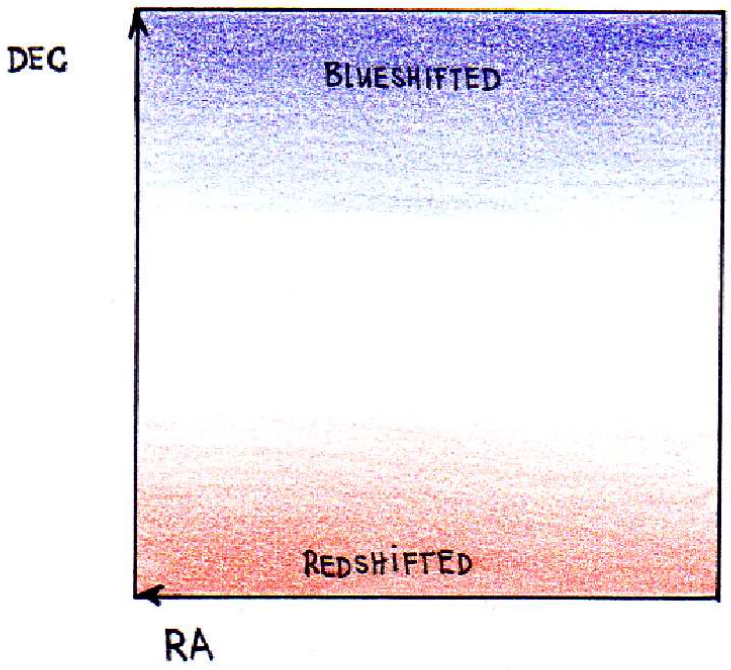

Figure 22: Map features

For the Kepler-Rotation model the top left hand side corner is the blue-shifted part and the bottom right hand side area is for redshifted velocities, as we will see in chapter: Interpretations of Kepler-Rotation Model - Results.

We know, that the outer peaks around $-5\,\frac{\text{km}}{\text{s}}$ and $5\,\frac{\text{km}}{\text{s}}$ (see fig. ((24) first plot, (26) last plot and accordingly (28) and (30)) are caused by the outflow, and the profile centre line is due to inflowing gaseous molecues. The reason for the left peak to be higher in brightness temperature we already discussed in a previous chapter.

The purpose of the next section is to interprete the maps of the velocity model profile of HCO^+ at different abundances for the outflow and the inflow region.

Maps are taken from eleven different velocity intervals:

$$\begin{aligned}
I_1 &= [-5.5, -4.5], \quad \text{average velocity} &&= -5\,\tfrac{\text{km}}{\text{s}} \\
I_2 &= [-4.5, -3.5], \quad \text{average velocity} &&= -4\,\tfrac{\text{km}}{\text{s}} \\
I_3 &= [-3.5, -2.5], \quad \text{average velocity} &&= -3\,\tfrac{\text{km}}{\text{s}} \\
I_4 &= [-2.5, -1.5], \quad \text{average velocity} &&= -2\,\tfrac{\text{km}}{\text{s}} \\
I_5 &= [-1.5, -0.5], \quad \text{average velocity} &&= -1\,\tfrac{\text{km}}{\text{s}} \\
I_6 &= [-0.5, +0.5], \quad \text{average velocity} &&= 0\,\tfrac{\text{km}}{\text{s}} \\
I_7 &= [+0.5, +1.5], \quad \text{average velocity} &&= +1\,\tfrac{\text{km}}{\text{s}} \\
I_8 &= [+1.5, +2.5], \quad \text{average velocity} &&= +2\,\tfrac{\text{km}}{\text{s}} \\
I_9 &= [+2.5, +3.5], \quad \text{average velocity} &&= +3\,\tfrac{\text{km}}{\text{s}} \\
I_{10} &= [+3.5, +4.5], \quad \text{average velocity} &&= +4\,\tfrac{\text{km}}{\text{s}} \\
I_{11} &= [+4.5, +5.5], \quad \text{average velocity} &&= +5\,\tfrac{\text{km}}{\text{s}}
\end{aligned} \tag{75}$$

I_1 to I_3 and I_9 to I_{11} the detected particles come from the outflow region. I_4 to I_8 are inflowing particles from the protostar.

From I_1 to I_3:
The geometrical graphic points out, that if particles (in our case HCO^+ molecules) have a velocity in the interval range of I_1 to I_3 , they come from the outflow region 1 if our line of sight is at an inclination of 25°. This conclusion is based on the knowledge that negative velocities correspond to a spectrum blue-shift and therefore molecules must approach us.

From I_9 to I_{11}:
Particles with energies between I_9 and I_{11} are also originated in an outflow region. Since their velocities are positive, their profile has to be redshifted. Thus region 3 is the only possible source where they may come from.

In our model the gas is not rotating, which implies that the intensity should be distributed symmetrically in the RA direction, while the declination (DEC) is positive for all blueshifted velocities, and negative for redshifted. If we look at the molecules which move perpendicular to our line of sight, there is no shift and therefore molecules have $v = 0\,\frac{\text{km}}{\text{s}}$.

How can be seen in the maps, that the blueshifted peak is bigger for the inflow and lower for the outflow region?

By looking at the maps (24) and (26) one can see, that the contour lines are less dense in the outflow region with average velocities of $-5\,\frac{\mathrm{km}}{\mathrm{s}}$ and $-4\,\frac{\mathrm{km}}{\mathrm{s}}$ than the positive average velocities of $+5\,\frac{\mathrm{km}}{\mathrm{s}}$ and $+4\,\frac{\mathrm{km}}{\mathrm{s}}$, where are higher intensity contour lines. It can even be seen in the optically thick map-spectra: (28) and (30) eventhough these effects are masked by others.

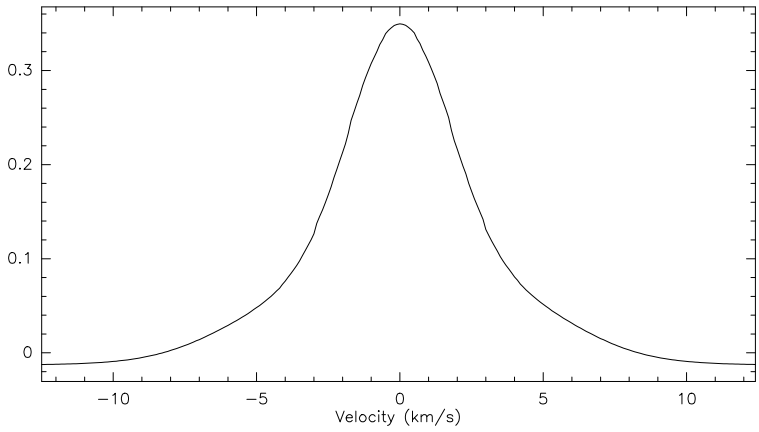

Figure 23: Optically thin temperature spectrum of the Velocity model

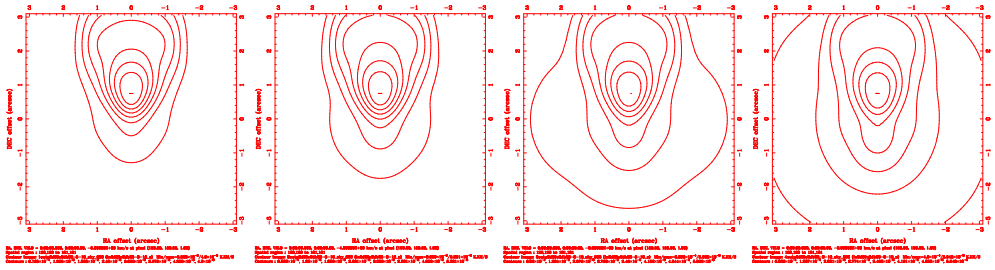

Figure 24: Intensity contour lines of the Velocity model with average velocity $= -5\,\frac{\text{km}}{\text{s}}$, $-4\,\frac{\text{km}}{\text{s}}$, $-3\,\frac{\text{km}}{\text{s}}$ and $-2\,\frac{\text{km}}{\text{s}}$, with beam convolution of 0.6

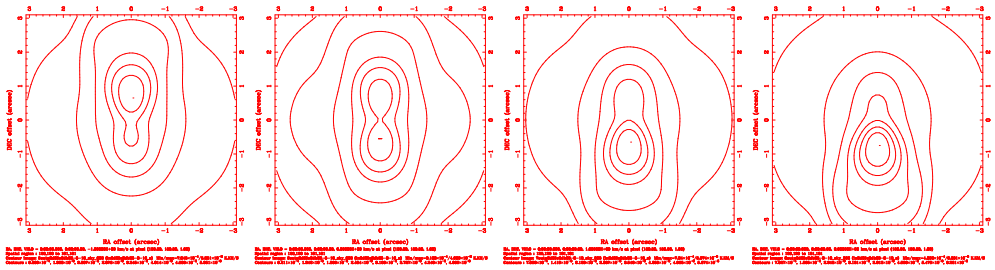

Figure 25: Intensity contour lines of the Velocity model with average velocity $= -1\,\frac{\text{km}}{\text{s}}$, $0\,\frac{\text{km}}{\text{s}}$, $1\,\frac{\text{km}}{\text{s}}$ and $2\,\frac{\text{km}}{\text{s}}$, with beam convolution of 0.6

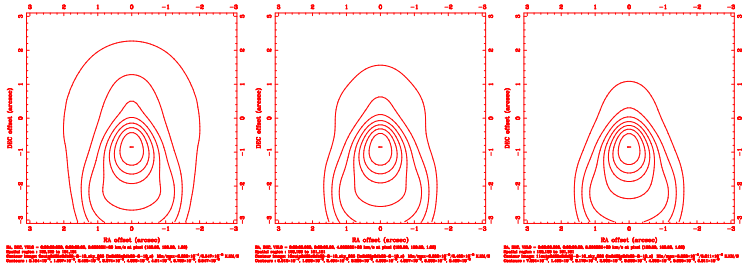

Figure 26: Intensity contour lines of the Velocity model with average velocity $= 3\,\frac{\text{km}}{\text{s}}$, $4\,\frac{\text{km}}{\text{s}}$ and $5\,\frac{\text{km}}{\text{s}}$, with beam convolution of 0.6

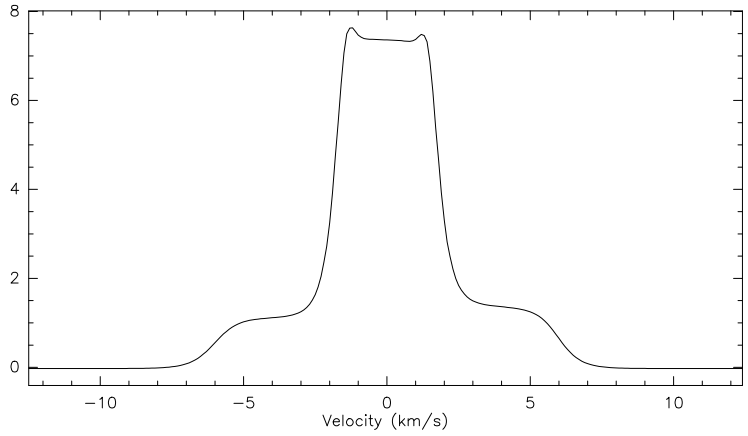

Figure 27: Optically thick temperature spectrum of the Velocity model

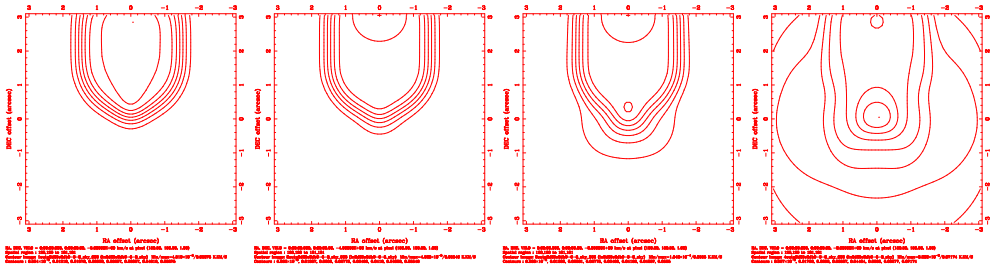

Figure 28: Intensity contour lines of the Velocity model with average velocity $= -5\,\frac{\text{km}}{\text{s}}$, $-4\,\frac{\text{km}}{\text{s}}$, $-3\,\frac{\text{km}}{\text{s}}$ and $-2\,\frac{\text{km}}{\text{s}}$, with beam convolution of 0.6

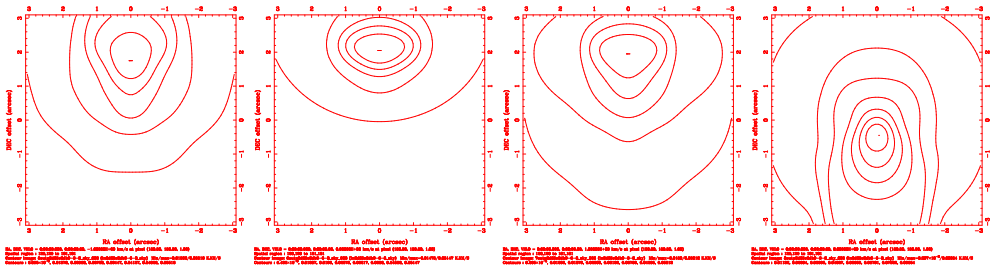

Figure 29: Intensity contour lines of the Velocity model with average velocity $= -1\,\frac{\text{km}}{\text{s}}$, $0\,\frac{\text{km}}{\text{s}}$, $1\,\frac{\text{km}}{\text{s}}$ and $2\,\frac{\text{km}}{\text{s}}$, with beam convolution of 0.6

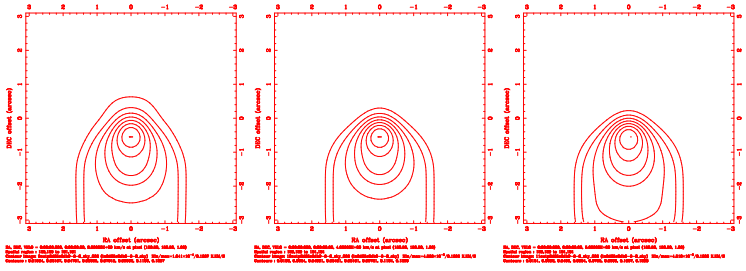

Figure 30: Intensity contour lines of the Velocity model with average velocity $= 3\,\frac{\text{km}}{\text{s}}$, $4\,\frac{\text{km}}{\text{s}}$ and $5\,\frac{\text{km}}{\text{s}}$, with beam convolution of 0.6

3.4 Kepler Model

In order to get a rotating velocity field, the Kepler velocity is taken for the azimuthal velocity vector v_a. Therefore v_r and v_z are zero in the inflow region and we set $v_r = 4\,\frac{km}{sec}$ in the outflow region and then separate it into two components v_r and v_z as we did in the former Velocity model. So v_a is defined as:

$$v_a = \sqrt{\frac{G \cdot M_a}{\sqrt{x^2 + y^2}}} \tag{76}$$

where x and y are the coordinates of the centre of each cell. M_a is the constant $15 \cdot 1.989 \cdot 10^{30}$ kg which is 15 times the mass of the sun and correspond to the mass of the protostar AFGL 2591.

3.5 Interpretations of Kepler-Rotation Model - Results

[Errata: The plots made using the Kepler velocity are not exactly accurate. The used velocities are $\sqrt{2}$ times higher than the ones calculated with the formula 76]

Fig. (31) shows a optically thin spectrum of a Kepler-velocity-model transition. The inclination is 25°, and all maps are convolved with a beam of size 0.6. It is obvious that for this model the contour lines can't be distributed symmetrically around the point of origin. The reason is the rotation of all particles in the same direction in the outflow region of the gas. By looking inclined into the inflow - quite near from the outflow region, we see particles from the outflow racing against us and therefore the spectrum is blueshifted. Such molecules come from the region where the declination is positive and also is the right ascension, if the rotation is counterclockwise. In the other region, where particles are moving away from us, they appear redshifted in the map and are therefore positioned in the negative RA and negative DEC corner of the coordinate system.

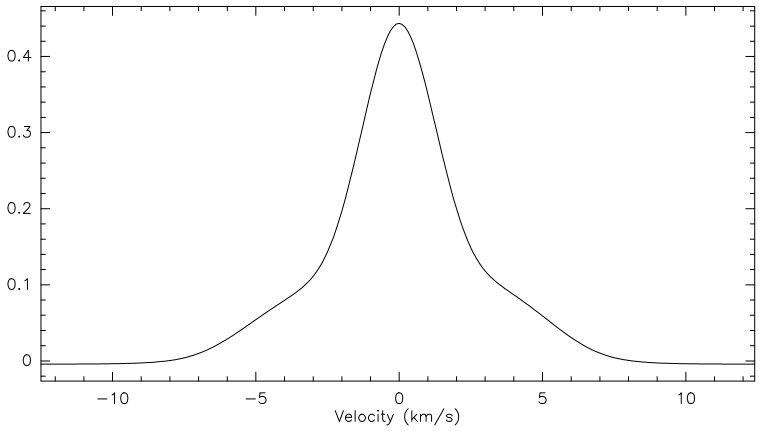

Figure 31: Optically thin temperature spectrum of the Kepler-Rotation model

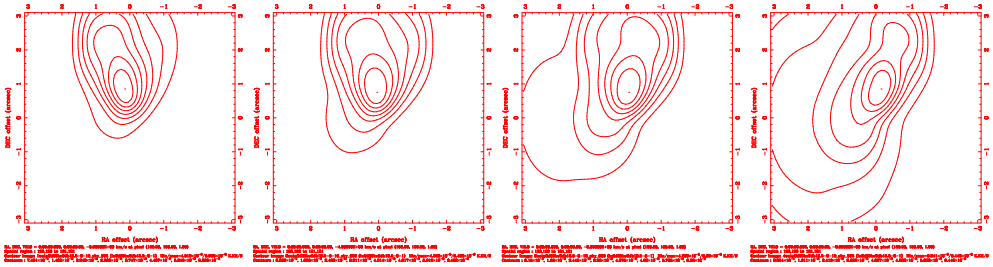

Figure 32: Intensity contour lines of the Kepler-Rotation model with average velocity $= -5\,\frac{\text{km}}{\text{s}}$, $-4\,\frac{\text{km}}{\text{s}}$, $-3\,\frac{\text{km}}{\text{s}}$ and $-2\,\frac{\text{km}}{\text{s}}$, with beam convolution of 0.6

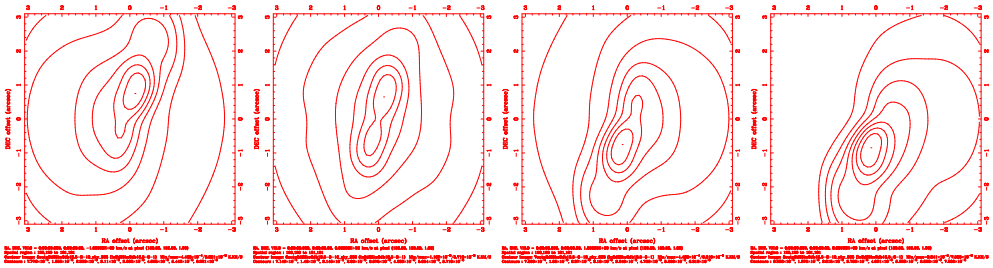

Figure 33: Intensity contour lines of the Kepler-Rotation model with average velocity $= -1\,\frac{\text{km}}{\text{s}}$, $0\,\frac{\text{km}}{\text{s}}$, $1\,\frac{\text{km}}{\text{s}}$, and $2\,\frac{\text{km}}{\text{s}}$, with beam convolution of 0.6

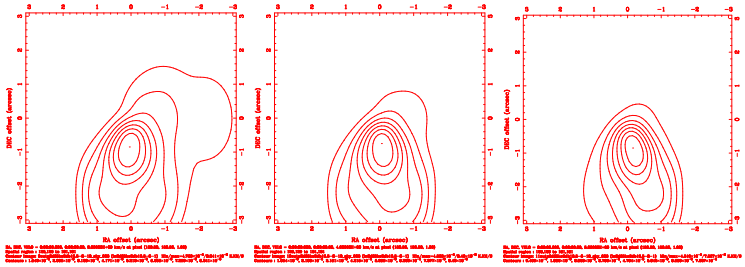

Figure 34: Intensity contour lines of the Kepler-Rotation model with average velocity $= 3\,\frac{\text{km}}{\text{s}}$, $4\,\frac{\text{km}}{\text{s}}$ $5\,\frac{\text{km}}{\text{s}}$, with beam convolution of 0.6

Quite conspicuous is the fact represented in fig. (32) to fig. (34), that the left hand outflow peak in the negative velocity range is slightly lower in temperature than the one in the redshifted area of I_9 to I_{11}. The explanation is similar to the explanation of the varying inflow peaks. (See chapter: Brightness temperature spectra and asymmetric lines) We still have an inclination of 25° onto the protostar. On account of this, molecules of region 1 are much more far away from the protostar than those particles which can be seen coming from the outflow region 3 (See fig. (6)).
The same effect can also be seen in fig. (35).

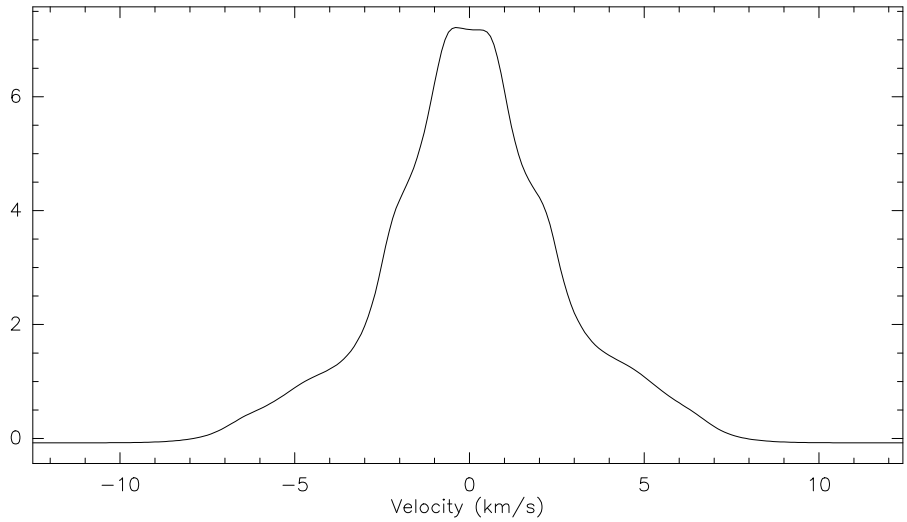

Figure 35: Optically thick temperature spectrum of the Kepler-Rotation model

I am very pleased, that I had this opportunity of working on the interesting topic of Ray-tracing in non-radial envelopes of Protostars at the ETH of Zurich. It was a great way of gaining an insight into the recent research of astrophysics. I learnt a lot and hope that I can continue learning in this exciting field of astrophysics.

4 Acknowledgements

Hereby I would like to say thank you very much to Arnold Benz for this great help whenever I requested it and for giving me this opportunity to work in his group. I'm also deeply grateful to Floris van der Tak who enabled me to in the first place do such a bachelor thesis by providing the amazing RATRAN 1d and 2d programs. I'm also grateful for his help. I also thank Pascal Stäuber for helping me and for all kind of programs he provided, which made my work much easier. To him and also to Paolo Grigis I would like to say thank you for the assistance whenever I had minor or major problems in programming or with astrophysical models. Sincere thanks go to Simon Bruderer for the support in the radiative transport chapter with his own Diploma thesis and to the great latex-help Felix Suwald.

References

[Acord et al. (1997)] J. M. Acord, E. Churchwell. The Extraordinary Outflow toward G5.89-0.39, Ap. J. 475:693-704, 1997

[Aikawa and Herbst (1999)] Y. Aikawa, E. Herbst. Molecular evolution in protoplanetary disks. Two-dimensional distributions and column densities of gaseous molecules, 1999, A&A 351,233

[Bachiller (1996)] R. Bachiller. Bipolar Molecular Outflows from Young Stars and Protostars, Annu. Rev. Astron. Astrophys. 34:111-54

[Charnley 1997] S. B. Charnley. *Sulfuretted Molecules in Hot Cores,* Ap.J.481:396-405, 1997

[Carroll, Ostlie (1996)] B. W. Carroll, D. A. Ostlie. Modern Astrpophysics, 1996

[Ceccarelli et al. (1996)] C. Ceccarelli, D. J. Hollenbach, A. G. G. M. Tielens. Far-Infrared Line Emission from Collapsing Protostellar Envelopes, ApJ 471, 1996

[Chiang and Goldreich (1997)] E. I. Chiang, P. Goldreich. Spectral Energy Distributions of T Tauri Stars with Passive Circumstellar Disks, ApJ 490,368, 1997

[Doty, Neufeld (1997)] S. Doty, D. Neufeld. Models for Dense Molecular Cloud Cores, ApJ 489, 1997

[Draine & McKee (1993)] B. T. Draine, C. F. McKee. Theory of interstellar shocks, Annu. Rev. Astron. Astrophys. 31:373-432, 1993

[Ehrenfreund et al. 1992] P. Ehrenfreund, R. Breukers, L. d'Hendecourt, J. M. Greenberg. On the possibility of detecting solid O2 in interstellar grain mantles, Astron. Astrophys. 260:431-36, 1992

[Gensheimer et al. (1996)] P. D. Gensheimer, R. Mauersberger, T. Wilson. Water in galactic hot cores, Astron. Astrophys. 314:281-94, 1996

[Genzel (1989)] R. Genzel. The Center of the Galaxy, ed. M.Morris, 393, 1989

[Genzel, Burton, Elmegreen (1991)] W. B. Burton, B. G. Elmegreen, R. Genzel. The Galactic Interstellar Medium, Saas-Fee Advanced Course 21, 1991

[Genzel et al. (1982)] R. Genzel, P. T. P. Ho, J. Bieging, D. Downes. NH3 in Orion-KL - A new interpretation, Ap. J. Lett. 259:L103-7, 1982

[Hartigan et al. (1991)] P. Hartigan, S. J. Kenyon, L. Hartmann, S. E. Strom, S. Edwards. Optical excess emission in T Tauri stars, Ap. J. 382:617-35, 1991

[Hasegawa, Herbst (1993)] T. I. Hasegawa, E. Herbst. Three-phase chemical models of dense interstellar clouds: Gas dust particle mantles and dust particle surfaces, Mon. Not. Roy.Astron. Soc. 263:589-606, 1993

[Hasegawa, Herbst (1993)] T. I. Hasegawa, E. Herbst. New gas-grain chemical models of quiescent dense interstellar clouds: The effects of H_2 tunneling reactions and cosmic rayinduced desorption, Mon. Not. Roy.Astron. Soc. 261:83-102, 1993

[Hogerheijde et al. (1998)] M. R. Hogerheijde, E. F. van Dishoeck, G. A. Blake, H. J. van Langevelde. Envelope Structure on 700 AU Scales and the Molecular Outflows of Low-Mass Young Stellar Objects, Ap. J.502:315, 1998

[Hogerheijde, van der Tak, (2000)] M. R. Hogerheijde, F. F. S. van der Tak. An accelerated Monte Carlo method to solve two-dimensional radiative transfer and molecular excitation, A&A 362,697-710, 2000

[Hollenbach (1997)] D. J. Hollenbach. In: Herbig-Haro Objects and the Birth of Low Mass Stars, ed. B. Reipurth, IAU Symp. 182, pp.181-98. Dordrecht: Kluwer, 1997

[Hollenbach & McKee (1989)] D. J. Hollenbach, C. F. Mc Kee. Molecule formation and infrared emission in fast interstellar shocks. III - Results for J shocks in molecular clouds, Ap. J. 342:306-36, 1989

[Hollenbach & Tielens (1989)] D. J. Hollenbach, A. G. G. M. Tielens. Dense Photodissociation Regions (PDRs), Annu. Rev. Astron. Astrophys. 35:179-216, 1997

[Jorgensen, Schöier and van Dishoeck (2003)] J. K. Jorgensen, F. L. Schöier, E. F. van Dishoeck. Molecular inventories and chemical evolution of low-mass protostellar envelopes, 2003, A&A 416,603-622(2004)

[Karttunen et al. (2001)] Karttunen et al., Tähtitieteen perusteet, Ursa, 2001, 3rd edition

[Lee et al. (1996)] H. H. Lee, R. P. A. Bettens, E. Herbst. Fractional abundances of molecules in dense interstellar clouds: A compendium of recent model results, Astron. Astrophys. Suppl. 119:111-14, 1996

[Mannings, Boss, Russel (2000)] V. Mannings, A. P. Boss, S. S. Russel. Protostars and Planets IV, Arizona 2000

[Mardones et al. 1997] D. Mardones, P. C. Myers, M. Tafalla, D. Willner, R. Bachiller, G. Garay. A Search for Infall Motions toward Nearby Young Stellar Objects, Ap. J. 489:719-33, 1997

[Millar et al. (1997)] T. J. Millar,M. S. El-Nawawy, D. A. Howe. Chemical evolution in collapsing cores, 1997

[Millar et al. (1997)] T. J. Millar, G. H. MacDonald, A. G. Gibb. A 330-360 GHz spectral survey of G 34.3+0.15. II. Chemical modelling, Astron. Astrophys. 325:1163-73, 1997

[Minh et al. (1990)] Y. C. Minh, W. M. Irvine, D. McGonagle, L. M. Ziurys. Observations of the H2S toward OMC-1, Ap. J. 360:136-41, 1990

[Minh et al. (1991)] Y. C. Minh, L. M. Ziurys, W. M. Irvine, D. McGonagle. Abundances of hydrogen sulfide in star-forming regions, Ap. J. 366:192-97, 1991

[Mitchell et al. (1990)] G. F. Mitchell, J. P. Maillard, M. Allen, R. Beer, K. M. Belcourt. Hot and cold gas toward young stellar objects, Ap. J. 363:554-73, 1990

[Mundy & McMullin (1997)] L. G. Mundy, J. P. McMullin. See van Dishoeck 1997, pp. 183-91, 1997

[Neufeld & Dalgarno (1989a)] D. A. Neufeld, A. Dalgarno. Fast molecular shocks. I - Reformation of molecules behind a dissociative shock, Ap. J. 340:869-93, 1989

[Neufeld & Dalgarno (1989b)] D. A. Neufeld, A. Dalgarno. Fast molecular shocks. II - Emission from fast dissociative shocks, Ap. J. 344:251-64, 1989

[Osterbrock (1974)] D. E. Osterbrock. Astrophysics of Gaseous Nebulae, Freeman, 1974

[Pauls et al. (1983)] A. Pauls, T. L. Wilson, J. H. Bieging, R. N. Martin. Clumping in Orion KL - 2-arcsecond maps of ammonia, Astron. Astrophys. 124:23-38, 1983

[Pelletier & Pudritz (1992)] G. Pelletier, R. E. Pudritz. Hydromagnetic disk winds in young stellar objects and active galactic nuclei, Ap. J. 394:117-38, 1992

[Rawlings et al. (1992)] J. M. C. Rawlings, T. W. Hartquist, K. M. Menten, D. A. Williams. Direct diagnosis of infall in collapsing protostars. I - The theoretical identification of molecular species with broad velocity distributions, MNRAS 255:471-85, 1992

[Rybicki & Hummer (1991)] G. B. Rybicki, D. G. Hummer. An accelerated lambda iteration method for multilevel radiative transfer,1991, A&A 245,171 Astrophysics of Gaseous Nebulae, Freeman, 1974

[Rybicki, Lightman (1979)] G. B. Rybicki, A. P. Lightman. Radiative processes in Astrophysics, 1979

[Sault et al. (1995)] R. J. Sault, P. J. Teuben, M. C. H. Wright. In: R. A. Shaw, H. E. Payne, J. J. E. Hayes. ASP Conf.Ser.77: Astronomical Data Analysis Software ans Systems IV, ASP, San Francisco, p.433, 1995

[Schöier, van der Tak, Dishoeck, Black (2004)] F. L. Schöier, F. F. S. van der Tak, E. F. van Dishoeck, J. H. Black. An atomic and molecular database for analysis of submillimetre line observations, 2004, astro-ph/0411110v

[Shepherd & Churchwell (1996)] D. S. Shepherd, E. Churchwell. Bipolar Molecular Outflows in Massive Star Formation Regions, Ap. J. 472:225-39, 1996

[Shu, (1977)] F. H. Shu. Self-similar collapse of isothermal spheres and star formation, ApJ 214,488,1977

[Shu et al. (1995)] F. H. Shu, J. Najita, E. C. Ostriker, H. Shang. Magneto-centrifugally Driven Flows from Young Stars and Disks. V. Asymptotic Collimation into Jets, ApJ 455:L155-58

[Spaans et al. (1995)] M. Spaans, M. R. Hogerheijde, L. G. Mundy, E. F. van Dishoeck. Photon Heating of Envelopes around Young Stellar Objects: an Explanation for CO J= 6–5, Ap. J. Lett. 455:L167-70, 1995

[Stahler, Palla (2004)] S. W. Stahler, F. Palla. The Formation of Stars, 2004

[Stäuber et al.] P. Stuber, S. D. Doty, E. F. van Dishoeck, A. O. Benz. X-ray chemistry in the envelopes around young stellar objects, Astron. Astrophys. 440:949-966, 2005

[Takahashi et al.,(1983)] T. Takahashi, J. Silk, D. J. Hollenbach. and thermal balance in a warm dusty medium, ApJ 275,145,1983

[Terebey et al. (1984)] S. Terebey, F. H. Shu, P. Cassen. The collapse of the cores of slowly rotating isothermal clouds, 1994, ApJ 286,529

[Tielens, Charnley (1997)] A. G. G. M. Tielens, S. B. Charnley. Circumstellar and interstellar synthesis of organic molecules, Origins Life Evol. Biosphere 27:23-51, 1997

[Tielens, Hagen (1982)] A. G. G. M. Tielens, W. Hagen. Model calculations of the molecular composition of interstellar rain mantles, 1982, Astron. Astrophys. 114:245-60

[van Langevelde,van der Tak (2004)] H. J. van Langevelde, F. F. S. van der Tak.
Radiation bookkeeping: a guide to astronomical molecular spectroscopy and radiative transfer problems with an emphasis on RADEX,
Bonn 2004

[van der Tak, van Dishoeck, Evans II, Bakker and Blake (1999)] F. F. S. van der Tak, E. F. van Dishoeck, N. J. Evans II, E. J. Bakker.
The impact of the massive young star GL 2591 on its circumstellar material: Temperature, density, and velocity structure, 1999,
The Astrophysical Journal, 522:991-1010

[van Dishoeck et al. (1998)] E. F. van Dishoeck, G. A. Blake.
Cemical evoltution of star-forming regions
(Annu. Rev. Astron. Astrophys. 1998, 36:317-68) 04, Vol.29, Issue 3, 359-366

[Wood & Churchwell (1989)] D. O. S. Wood, E. Churchwell.
Massive stars embedded in molecular clouds - Their population and distribution in the galaxy
Ap. J. 340:265-72, 1989

A Plot features

Figure:	(4)
Model:	non-velocity, 1- dimensional
Inflow density ratio:	10^{-10}
Outflow density ratio:	10^{-10}
Molecule:	HCO^+
Transition of the molecule:	$5 \rightarrow 4$
Inclination:	$0°$
SNR:	10

Figure:	(5)
Model:	Velocity
Inflow density ratio:	10^{-8}
Outflow density ratio:	10^{-8}
Molecule:	HCO^+
Transition of the molecule:	$4 \rightarrow 3$ and $5 \rightarrow 4$
Inclination:	$0°$
SNR:	5

Figure:	(7)
Model:	non-velocity, 2- dimensional
Inflow density ratio:	10^{-10}
Outflow density ratio:	10^{-10}
Molecule:	HCO^+
Transition of the molecule:	$4 \rightarrow 3$ and $5 \rightarrow 4$
Inclination:	$0°$
SNR:	10

Figure:	(8)
Model:	non-velocity, 1- dimensional
density ratio:	10^{-10}
Molecule:	HCO^+
Transition of the molecule:	$4 \rightarrow 3$ and $5 \rightarrow 4$
Inclination:	$0°$
SNR:	10

Figure:	(9)
Model:	non-velocity
Inflow density ratio:	10^{-10}
Outflow density ratio:	10^{-10}
Molecule:	HCO^+
Transition of the molecule:	$6 \rightarrow 5$ and $8 \rightarrow 7$
Inclination:	$0°$
SNR:	10

Figure:	(10)
Model:	Velocity
Inflow density ratio:	10^{-8}
Outflow density ratio:	10^{-4}
Molecule:	HCO^+
Transition of the molecule:	$4 \rightarrow 3$
Inclination:	$0°$
SNR:	5

Figure:	(11)
Model:	Kepler-Rotation model without and with inflow
Inflow density ratio:	10^{-8}
Outflow density ratio:	10^{-8}
Molecule:	HCO^+
Transition of the molecule:	$4 \rightarrow 3$
Inclination:	$0°$
SNR:	5

Figure:	(12), (13), (14)
Model:	Velocity
Inflow density ratio:	10^{-8}
Outflow density ratio:	10^{-8}
Molecule:	HCO^+
Transition of the molecule:	$4 \rightarrow 3$
Inclination:	$0°$, $15°$, $25°$
SNR:	5

Figure:	(15), (16), (17)
Model:	Velocity
Inflow density ratio:	10^{-8}
Outflow density ratio:	10^{-8}
Molecule:	HCO^+
Transition of the molecule:	$4 \rightarrow 3$
Inclination:	30°, 45°, 60°
SNR:	5

Figure:	(18), (18), (19), (20)
Model:	Velocity
Inflow density ratio:	10^{-8}
Outflow density ratio:	10^{-8}
Molecule:	HCO^+
Transition of the molecule:	$4 \rightarrow 3$
Inclination:	25°
SNR:	5

Figure:	(21)
Model:	Velocity
Inflow density ratio:	10^{-10}
Outflow density ratio:	10^{-8}
Molecule:	HCO^+
Transition of the molecule:	$4 \rightarrow 3$
Inclination:	25°
SNR:	5

Figure:	(23) - (26)
Model:	Velocity, optically thin
Inflow density ratio:	10^{-10}
Outflow density ratio:	10^{-8}
Molecule:	HCO^+
Transition of the molecule:	$4 \rightarrow 3$
Inclination:	25°
SNR:	5

Figure:	(27) - (30)
Model:	Velocity, optically thick
Inflow density ratio:	10^{-8}
Outflow density ratio:	10^{-6}
Molecule:	HCO^+
Transition of the molecule:	$4 \rightarrow 3$
Inclination:	$25°$
SNR:	5

Figure:	(31) - (34)
Model:	Kepler-Rotation
Inflow density ratio:	10^{-10}
Outflow density ratio:	10^{-8}
Molecule:	HCO^+
Transition of the molecule:	$4 \rightarrow 3$
Inclination:	$25°$
SNR:	5

Figure:	(35)
Model:	Kepler-Rotation
Inflow density ratio:	10^{-8}
Outflow density ratio:	10^{-6}
Molecule:	HCO^+
Transition of the molecule:	$4 \rightarrow 3$
Inclination:	$0°$
SNR:	5